QUANTITATIVE METRICS OF SOIL STRUCTURE AND RELATIONSHIPS TO HYDRAULIC PROPERTIES IN A VERTIC ARGIUDOLL

BY

Dennis Vernon Eck

Submitted to the graduate degree program in Geography and the Graduate Faculty of the University of Kansas in partial fulfillment of the requirements for the degree of Master of Science.

_____

Chairperson Daniel R. Hirmas

_____

Nathaniel A. Brunsell

_____

William C. Johnson

Date Defended: March 11, 2014

The Thesis Committee for Dennis V. Eck
certifies that this is the approved version of the following thesis:

QUANTITATIVE METRICS OF SOIL STRUCTURE AND RELATIONSHIPS TO HYDRAULIC PROPERTIES IN A VERTIC ARGIUDOLL

_____

Chairperson Daniel R. Hirmas

Date Defended: March 11, 2014

ABSTRACT

Soil structure is a fundamental property referring to the morphology of soil aggregates and the network of void spaces between them. Structure affects many pedogenic, hydrological, and other ecosystem service processes. While its importance is generally recognized, the tortuous nature of soil structure and its variable size and expression make this property difficult to quantify, especially at the pit scale. The absence of quantitative soil structure metrics also inhibits the ability to accurately model water flux. This research explores the application of multistripe laser triangulation (MLT) scanning to a soil profile in the field. MLT scan data were analyzed for their ability to quantitatively characterize soil structure. The study site was located near Lawrence, KS in a Grundy soil series with vertic properties, where soil moisture sensors were installed in a lysimeter next to an exposed profile. Several logistical problems concerning MLT field operations and data processing are addressed in this work including: ambient light, MLT scanner positioning in relation to the soil surface, and post-processing procedures for the resulting data. MLT scans capture the profile surface along with areas of missing data, termed surface scan gaps (SSGs), which represent preferential flow paths (PFPs) actually observed in the soil. Metrics describing SSGs were first studied to determine whether the digital data could be related to conditions observed in the field. These metrics were then examined in relation to soil hydraulic parameters, especially saturated hydraulic conductivity (K_s) and water retention curve (WRC) parameters. Soil moisture data collected at the lysimeter, in conjunction with atmospheric data from an adjacent tower, were used as inputs for Hydrus 1-D to predict, then separately to verify hydraulic parameters that were obtained using quantitative soil structure metrics. Several close relationships were identified with WRC parameters such as α and n, as well as relationships with K_s. These connections, enabled by quantification of soil structure as a

continuous rather than categorical variable through field-based measurements, present an opportunity to inform soil water flux models and advance the understanding of mechanisms underlying field-scale cycling of soil water.

ACKNOWLEDGEMENTS

After completing a project of this magnitude, there are many people who are owed debts of gratitude. I am especially thankful to my advisor, Dr. Dan Hirmas. He has patiently given encouragement and guidance throughout these years of research, which spread well beyond the boundaries of this work, ensuring the completion of this ambitious project and augmenting my education in multiple ways. Many thanks also to Dr. Nate Brunsell and Dr. Bill Johnson for their service as committee members. They graciously contributed support and insight throughout the research and writing processes. Additional expertise contributed by Dr. Daniel Giménez, to whom I am very grateful, improved the final product substantially and greatly eased the peer-review process for publication. I am thankful for the assistance of Dr. Dean Kettle and Bruce Johanning at the KU Field Station. Aaron Koop also provided invaluable help in the field along with constant support and confident optimism. Thanks are also due to Leiqiu Hu and Eric Zautner as well as Dr. Brian Platt for their help with various aspects of this work. This research was supported in part by the University of Kansas General Research Fund and the Kollmorgen Fellowship Fund, for which I am grateful. The study was conducted at and supported in part by the University of Kansas Field Station, a research unit of the Kansas Biological Survey and the University of Kansas. I am also grateful for the support and accommodation provided by the Field Station. I am profoundly indebted to my family for their constant faith, love, support and humor through the trials and tribulations of graduate school. My dad, Larry Eck, provided hours of assistance with laboratory work during his highly-valued time off work, for which I am exceedingly grateful. Finally, I give my deepest thanks to Anna Johnson, whose love and support have made the completion of this work even more fulfilling. This work is dedicated to our child, whose arrival will begin a completely new kind of lifelong education.

TABLE OF CONTENTS

CHAPTER 1. INTRODUCTION

Soil structure refers to the size, shape, and expression of peds, along with the coincident network of interpedal pore spaces (Hillel, 1998). While it is widely recognized as a fundamental soil property affecting pedogenic, hydrological and environmental processes and behavior, the tortuous nature and spatio-temporal heterogeneity of soil structure make it a difficult property to describe quantitatively. Until recently, it has been described qualitatively in the field based on the judgment of the observer. As a qualitative variable, it is subject to the challenges and limitations of maintaining uniformity and agreement when shared among multiple observers. Additionally, the usefulness of these field-based qualitative descriptions of soil structure to modeling soil physical processes such as water flux is hindered by the discrete nature of the categories assigned. What is needed, therefore, is an objective and quantitative description of soil structure and pore networks characterized by parameters that vary over a continuous scale.

The recent development of multistripe laser triangulation (MLT) provides the opportunity to investigate the application of a structured-light scanning technique to quantitatively characterize soil structure in the field. MLT has already been employed in measuring soil bulk density (Rossi et al., 2008), characterizing ichnofossils (e.g., Platt et al., 2010), and digitizing archaeological artifacts (e.g., DeSilva, 2009, Clarkson and Hiscock, 2011, Sholts et al., 2012). While the utility of MLT scanning is known in a variety of disciplines, there is a lack of research applying the technology to quantitative characterization of soil profiles. Yet, the advantages of MLT include the potential to obtain quantitative data in the field rather than the laboratory and at a relatively low cost. Several logistical challenges exist to applying MLT to soil profiles in the field such as ideal scanning conditions, profile face conditions necessary for collecting high quality data and best practices in post-processing the resulting data. These challenges of

acquiring MLT data in the field and identifying the appropriate data processing operations are the focus of Chapter 2. This research was carried out at the Nelson Environmental Study Area (NESA) at the University of Kansas Field Station (KUFS). A passive capillary lysimeter was installed along with 5 soil moisture and temperature sensors to continuously monitor conditions throughout the study period. The study site was located adjacent an Ameriflux eddy covariance tower to allow for the incorporation of atmospheric variables and promote future work combining the two data sets. Various quantitative metrics were obtained from the MLT digital data and several new metrics were calculated. The resolution of these questions allowed the resulting quantitative characterizations to be related to soil hydraulic parameters. Chapter 3 describes those analyses investigating whether relationships exist between water flux and the measured data. Soil moisture and atmospheric data were used as inputs for Hydrus 1-D (Šimůnek et al., 2013), which was utilized to solve for soil hydraulic parameters. Results of this research demonstrate the feasibility of applying MLT scanning to quantitative characterization of soil structure and the utility of the resulting data in predicting soil hydraulic properties.

REFERENCES

Clarkson, C., and P. Hiscock. 2011. Estimating original flake mass from 3d scans of platform area. Journal of Archaeological Science 38:1062-1068.

DeSilva, J.M. 2009. Functional morphology of the ankle and the likelihood of climbing in early hominins. Proceedings of the National Academy of Sciences 106:6567-6572.

Hillel, D. 1998. Environmental soil physics. Academic Press, New York.

Platt, B.F., S.T. Hasiotis, and D.R. Hirmas. 2010. Use of low-cost multistripe laser triangulation (MLT) scanning technology for three-dimensional, quantitative paleoichnological and neoichnological studies. Journal of Sedimentary Research 80:590-610.

Rossi, A.M., D.R. Hirmas, R.C. Graham, and P.D. Sternberg. 2008. Bulk density determination by automated three-dimensional laser scanning. Soil Science Society of America Journal 72:1591-1593.

Sholts, S.B., D.J. Stanford, L.M. Flores, and S.K.T.S. Wärmländer. 2012. Flake scar patterns of Clovis points analyzed with a new digital morphometrics approach: Evidence for direct transmission of technological knowledge across early North America. Journal of Archaeological Science 39:3018-3026.

Šimůnek, J., M. Šejna, H. Saito, M. Sakai, and M. Th. van Genuchten, The Hydrus-1D Software Package for Simulating the Movement of Water, Heat, and Multiple Solutes in Variably Saturated Media, Version 4.16, HYDRUS Software Series 3, Department of Environmental Sciences, University of California Riverside, Riverside, California.

CHAPTER 2. QUANTIFYING SOIL STRUCTURE FROM FIELD EXCAVATION WALLS USING MULTISTRIPE LASER TRIANGULATION SCANNING

ABSTRACT

Soil structure is fundamental for understanding pedogenic, hydrological, and environmental processes and its quantitative characterization essential for advancing our understanding of soils. Despite this importance, quantification of structure at scales relevant to field-based investigations has remained elusive. In this study, multistripe laser triangulation (MLT) scanning was investigated as a method for quantifying soil structure from excavation walls. An exposed soil profile in a Grundy soil series (fine, smectitic, mesic, Oxyaquic Vertic Argiudoll) was scanned using a commercially available MLT scanner. Scanning was done at night to avoid complications from ambient light and temperature and water fluxes at the profile surface. The field of view (FOV) for each scan overlapped with adjacent scan FOVs by approximately 10 cm in the vertical and horizontal directions. The data of interest for the MLT scans were areas where laser stripes were not detectable by the scanner. These surface scan gaps (SSGs) are narrow and deep areas outlining structural units. We discovered that the angle between the scanner and the excavation wall produces significant differences between the resulting image data and that merging data into a single digital mesh (a very time consuming post-processing option) is unnecessary as it produced no differences from unmerged data. Observed SSGs best represented structure outlines on the left side of the scan data FOVs; right sides were greatly improved by complementing data obtained from the left sides of overlapping FOVs. Several metrics describing SSG shape, size, and orientation were produced. SSG density, SSG fraction, relative surface area, and average unit size (i.e., size of areas outlined by

SSGs) were related to soil structure described in the field. MLT scanning holds potential for quantitative characterization of soil structure with implications for water flux modeling and advancing understanding of pedological and hydrological processes.

INTRODUCTION

Soil structure describes the shape, expressive strength, and size of peds at meso- and macro-scales and the resulting network of interpedal pore spaces (Hillel, 1998). Structure often reflects the pedogenic history of a soil and interacts with soil forming processes that shape soil development. Interpedal pores are important because they can control preferential flow and transport since these pores provide pathways for water to bypass matrix flow. Better characterization of soil structure at scales that are relevant to resource management is an essential need for advancing our understanding of soil processes at the field scale (McKenzie, 2006; Lin, 2010).

Several methods have previously been applied to characterize soil structure and interpedal pores (e.g., traditional morphological description, dye studies, measurement from sensors and lysimeters, smoke injection), but these methods can only obtain estimates of structure (Allaire et al., 2009). There are also numerous descriptive and semi-quantitative methods for characterizing and scoring soil structure by visual inspection (e.g., Peerlkamp, 1967; Batey, 2000; McKenzie, 2001). The profile development index proposed by Harden (1982) produces a semi-quantitative metric for soil structure by using a rubric to assign values on an arbitrary scale to structure described qualitatively in the field. This system creates numerical values that generally characterizes the sequence of soil development, but does not quantitatively describe structure per se. Lepore et al. (2009) recently advanced a more sophisticated method by

considering structure size (which is based on an underlying continuous distribution) as well as structural grade in their characterization of simplified soil structure geometries for water flux modeling purposes. This method must still rely on qualitative descriptions (which are subject to investigator bias) to parameterize soil structure in the absence of direct measurement techniques for quantitative soil structure characterization. Another method was recently developed to cast macropores with liquid latex in situ (Abou Najm et al., 2010), but this method requires labor-intensive excavation of the cast and provides little quantitative data.

By contrast, multistripe laser triangulation (MLT) scanning, a type of structured light scanning, obtains quantitative data of scanned surfaces. Recent work has utilized MLT scanning in quantitative applications such as measuring bulk density of soil (Rossi et al., 2008), measuring shape, surface area, and volume of rocks (Rossi and Graham, 2010; Asahina and Taylor, 2011), characterizing shapes and volumes of ichnofossils and terrestrial traces (Platt et al., 2010; Adams et al., 2010; Wright and Selden, 2011), quantitatively characterizing various skeletal morphologies in archaeological studies (e.g., DeSilva, 2009; DeSilva, 2010; Sholts et al., 2010; Barney et al., 2012), digitally capturing and characterizing high-quality archaeological artifacts (Abate et al., 2011; Sholts et al., 2012), and predicting flake mass produced during stone toolmaking (Clarkson and Hiscock, 2011). The performance of MLT scanners compares reasonably well with other types of scanners (Guidi et al., 2007), particularly for morphometric procedures (Sholts et al., 2011). MLT scanners have also been favorably compared to X-ray computed tomography (Asahina and Taylor, 2011) although a recent study has noted issues of uncertainty and repeatability in the scanned data (Polo and Felicisimo, 2012).

The potential of MLT scanning as an accurate, field-portable tool has been identified, but its deployment in the field presents several challenges. While there is a growing body of

literature about MLT and other structured light scanning techniques, we are unaware of recommendations directly relevant to the scanning of excavation walls. Outstanding questions include space requirements, temperature limitations, and conditions of the excavation wall necessary to obtain high-quality digital data. Digital data requires processing after collection, but the effects of different post-processing procedures on the digital data are also unknown.

While MLT scanning is designed to collect data on solid surfaces, we hypothesized that, if applied to a soil profile, gaps in the resulting scan data could outline soil structural units, making quantitative characterization possible. Thus, we investigated the use of MLT scanning in the field at the pit scale. Specific objectives were to: (1) develop methods for scanning an excavated soil profile in the field and (2) apply the resulting digital data to characterize structural units. If this technique were successful in characterizing soil structural units, it would have potential application in pedological investigations and could assist in the parameterization of preferential flow models.

MATERIALS AND METHODS

Study site

Fieldwork was conducted in the Nelson Environmental Study Area (NESA) at the University of Kansas Field Station (KUFS), Jefferson County, Kansas. NESA is located in a tallgrass prairie upland with an average annual temperature of 12°C and average annual precipitation of 914 mm. The site, located in a tallgrass prairie and oak-hickory forest ecotone (Kettle et al., 2000), is covered mainly by native grasses such as big and little bluestem, Indian grass, and switch grass. It is managed by mowing and occasional burning to control woody encroachment (D. Kettle, personal communication, 2012).

Field sampling

A 1-meter soil profile was exposed in a summit position of the Grundy soil series (fine, smectitic, mesic, Oxyaquic Vertic Argiudoll; Soil Survey Staff, 2012) and described following Schoeneberger et al. (2002). Bulk density samples were collected in triplicate with 3 cm x 5.4 cm (i.d.) brass rings from each horizon using a soil sampler (SoilMoisture Equipment Corp, Santa Barbara, CA). We removed artificial roughness imparted on the profile surface from cleaning tools by freezing and peeling the excavation face, following the method developed by Hirmas (2013). Before collecting digital data with the MLT scanner (NextEngine Desktop 3D Scanner Model 2020i, NextEngine, Inc., Santa Monica, CA), the pit was allowed to dry for 36 hours to enhance the visible appearance of soil structure. A tape measure was placed near the edge of the prepared face and colored ball-head pins were pushed into the excavation wall at 10-cm depth intervals spanning the profile width, creating a reference system to align and georeference the digital data.

A portable generator (Inverter EF1000iS, Yamaha, Hamamatsu, Shizuoka, Japan) coupled with a 330V transient suppressed voltage surge protector (Model 958-893, Ativa, Boca Raton, FL) provided steady power needed to use the laptop and scanner in the field. The MLT scanner was positioned at the bottom of the pit 43 cm from the excavation wall, per manufacturer recommendations, and leveled. Scans were collected at the highest resolution (150 DPI), beginning with the bottom left side of the exposed face (Fig. 1; bottom left scan). Parallel vertical laser stripes become deformed as they are swept across the surface of interest, and distances are computed by variations in light intensity of the projected laser stripes detected by the scanner (Knighton et al., 2005; Platt et al., 2010). Since the field of view (FOV) of the scanner was narrower than the prepared section of excavation wall, the scanner was moved to the

right side of the excavation wall after the initial scan (Fig. 1; bottom right scan). A second scan was collected at the same height and distance from the pit face as the previous scan. Adjacent FOVs overlapped by approximately 10 cm (Fig. 1; bottom scans). A telescoping tripod was used to reposition the scanner above the first digital profile segment with 5-10 cm of vertical overlap, where a third scan was collected (Fig. 1; top left scan). It was then moved to the right side at the same height (Fig. 1; top right scan) with approximately 10 cm of (horizontal) overlap with the adjacent scan (Fig. 1; top scans) and 10 cm (vertical) overlap with the scan below (e.g., Fig. 1; right scans), and the fourth scan was collected (Fig. 1; top right scan). This procedure was continued until the remainder of the profile was collected. Resulting surface scans, each producing a triangulated irregular network (TIN), were saved to a single file.

Laboratory Analyses

Particle–size distribution was determined with the pipette method (Gee and Or, 2002) after pre-treatment to remove organic matter. Bulk density was determined from the sampled cores following Grossman and Reinsch (2002). Organic and inorganic carbon content were measured with a coulometer (CM5015, UIC Inc., Joliet, IL) following Jackson and Roof (1992) and Engleman (1985), respectively.

The data of interest for the MLT scans were actually the missing data in the original surface scans (i.e., where the laser stripes were not detectable by the scanner), referred to herein as surface scan gaps (SSGs). Files from MLT scans contained a separate TIN mesh from each scan position. Photographs captured by the scanner at the beginning of each scan (Fig. 2a) were removed from the file. Digital data were processed in ScanStudio HD (NextEngine Inc., Santa Monica, CA).

An area covered by four overlapping scans within a depth of 61-85 cm (Fig. 1) was examined for effects caused by digital data post-processing treatments applied to 14 separate combinations of scan positions and post-processing treatment (Fig. 3). These overlap configurations consisted of stacked (i.e., multiple scans overlain similar to overlain transparencies), and merged (i.e., multiple scans combined by the software into a single mesh) post-processing treatments in addition to the four individual scans (Fig. 1; overlap configurations K-N were not merged since each is a single mesh). Figure 2b is an example of the visual results of post-processing. Images for horizons (n = 7) were processed in a manner similar to the overlap test (Fig. 3).

Histograms of SSG size and shape parameters measured for the 61-85 cm depth were visually inspected for normality. Pairwise *t*-tests were performed between each of the 14 data configurations for the same measured SSG parameters to assess the results of the overlap test. Family-wise error rates were accounted for using the Bonferroni method (Logan, 2010) and results were plotted in a visual matrix. All statistical data analyses were performed using R (R Development Core Team, Vienna, Austria).

RESULTS AND DISCUSSION

Measured Data

Results of the field morphological description and selected physical properties from each of the seven horizons are shown in Table 1. The upper five horizons formed in loess and, below the lithologic discontinuity at 61 cm, the lower two horizons formed in glacial till. Direct evidence of glacial till was not observed in the Btss1 horizon but the presence of slickensides as well as similar particle-size distribution (and same texture) to the horizons below indicate the

Btss1 derived some physical characteristics from the same glacial till parent material as the 2Btss2 and 2Btss3. While clay content increases with depth throughout the profile, it increases more than 13% from the Bt2 to the Btss1 horizon, just above the lithologic discontinuity (Table 1). Changes in the appearance of structural features below 54 cm, with generally larger and better defined peds dominating the three lower horizons (Fig. 2), correspond with these measured physical properties of the soil profile.

Missing data in the original surface scans, or SSGs, correspond to relatively narrow and deep gaps in the soil fabric at the exposed profile surface. Based on field observation and visual inspection, SSGs are assumed to represent spaces between structural units because the surface was carefully cleaned following Hirmas (2013), thus reducing artificial shadowing effects. Since those areas initially invisible to the scanner (i.e., SSGs) outline soil structures, they allow structure to be analyzed indirectly.

We directly measured parameters describing size and shape (Table 2) for each individual SSG in ImageJ (Research Services Branch, National Institute of Health, Bethesda, MD). These measurements were taken for all horizons and overlap configurations. Histograms of resulting measurements revealed that the data were not normally distributed. Logarithmic transformations produced distributions that were more normal and resulted in considerably different mean values from the respective untransformed means. We normalized circularity (C) using a log [log (1 / C)]-transformation. Distributions of untransformed data were generally highly skewed and over-predicted mean values. No transformation was applied to roundness since untransformed data already displayed characteristics of a normal distribution.

Overlap Test

In general, an area scanned from different positions will vary when the surface (e.g., an excavation wall) has some topographic relief. This variation can be explained by the orientations of the MLT laser source, camera window, and the excavation wall (Fig. 1). One area from the 2Btss2 horizon where four individual scans overlapped was examined to ascertain whether significant differences exist between the 14 overlap configurations (Fig. 1). When scanning the overlap area from the left position of the prepared excavation wall, the angle β in Fig. 1 (scanner position a), defined by a line between the camera window and the right side of the FOV, is acute. The angle γ in Fig. 1 (scanner position a), defined by a line extending from the laser source to the right side of the FOV, is approximately perpendicular to the face of the scanner. By contrast, this relationship is reversed when collecting the overlapping area from the right position of the wall, with β (camera view angle) at nearly 90° while γ (laser source angle) is acute (Fig. 1; scanner position b). Visual analysis of the resulting images reveals the effects of data composition (i.e., combination of scans collected from different positions) on the apparent sizes of SSGs (Fig. 4). Holding post-processing treatment (i.e., stacked vs. merged) constant, SSGs appear larger in the images from the left scan positions ($\beta < 90°$; $\gamma \sim 90°$) and top scans (e.g., Fig. 4; overlap configurations G and K) compared to the smaller appearance in right scans ($\beta \sim 90°$; $\gamma < 90°$; e.g., Fig. 4; overlap configuration J) and bottom scans. The apparent continuity and number of SSGs seem to be more affected by the post-processing treatment, although the effect is not consistent. Some overlap configurations show more SSGs in merged as opposed to stacked treatments (e.g., Fig. 4; overlap configurations A vs. J) while others exhibit more but less continuous SSGs in stacked as opposed to merged configurations.

Shadowing tends to exaggerate the size of SSGs in the images, so the best representation of the actual condition of the excavation wall is most likely the smallest and least exaggerated image. Using this criterion, the scanner performs best when $\beta \sim 90°$ and $\gamma < 90°$ as demonstrated by configuration A in Fig. 4. In practice, the least accurate data collected appears to be the area between the right edge of the FOV and directly in front of the scanner. It is necessary, therefore, to collect overlapping data to achieve the best accuracy for areas at least as wide as a single FOV; this overlap width should be ~10 cm or greater. In our study, the overlap area covers the least accurate portion of the left side scan ($\beta < 90°$; $\gamma \sim 90°$).

We contrasted 11 parameters defining the SSG morphology across each of the 14 overlap configurations using pairwise *t*-tests. Results were plotted as a star plot matrix with each slice representing the $1 - P$ value for that parameter (Fig. 5). The radius of rings, plotted for each star plot, represent a $1 - \alpha$ distance of 0.95 from the center of the plot. Slices that extend to the ring or beyond indicate a significant difference with respect to that parameter between the overlap configurations being contrasted. Perhaps the most important outcome is that results from the overlap configurations A (all scans stacked) and B (all scans merged) are not significantly different from each other. When constructing a full digital soil profile, merging pit face scans required a substantial amount of computing time (more than 2 hours per alignment in some cases). Since A and B are not significantly different, merging the data can be avoided which saves a considerable amount of time during post-processing. Comparisons of rows B-J to overlap configurations A and B show that with all else constant, the overlap areas captured from the right scan position ($\beta \sim 90°$; $\gamma < 90°$) and bottom scan positions are more similar to A and B than overlap areas from left ($\beta < 90°$; $\gamma \sim 90°$) and top scan positions (Fig. 5; overlap configurations A/F and B/F vs. A/D and B/D; A/J and B/J vs. A/H and B/H). Even when right or

bottom scans have significant differences for some parameters, more differences emerge in the left and top scans, although they are not necessarily statistically significant (e.g., Fig. 5; overlap configurations A/E and B/E vs. A/C and B/C). Comparisons of columns C – I down to row J also show more significant differences in top and left positions (e.g., Fig. 5; overlap configurations C/J and D/J vs. E/J and F/J). Comparisons of individual scans follow the same pattern, with significant differences in more parameters for the top and left positions than bottom and right positions (e.g., Fig. 5; overlap configurations C/L and D/L vs. C/K and D/K).

To further analyze these differences, boxplots for all 14 configurations were created for selected parameters (Fig. 6). In nearly all cases, the spread of the data was greater for the merged treatment than for the stacked treatment. The low median values for the stacked data were taken to be a better representation of the actual condition of the excavation wall since any shadowing effects during scanning (arising from irregularities in the topography of the excavation wall; see Fig. 2) still present after preparation of the profile would enlarge the apparent size of the SSGs. From these analyses, we concluded that merging the data is unnecessary and, due to the greater amount of this noise, may be less accurate than using the stacked data. As discussed previously, this greatly reduces the time required for post-processing scan data. Within the overlap area, data collected from the left scans had more noise than the right scans (Fig. 6), again suggesting that scan data toward the right edge of a given FOV (Fig. 1a; $\beta < 90°$; $\gamma \sim 90°$) is the least accurate and should be supplemented by data from the left side (Fig. 1b; $\beta \sim 90°$; $\gamma < 90°$) of an overlapping FOV.

Based on results from this overlap test, we used stacked data and cropped the digital profile to the FOV of the left scans (e.g., Fig. 1K, M), taking care to include the overlapping data

from the right scans. Combining scans from more than one position helps to improve quality and remove noise and systematic errors in the scan data (Abbasinejad et al., 2009).

Structural Metrics, Soil Properties and Morphology

Differences between horizons were quantified with composite measurements (Table 2) and plotted by depth (Fig. 7). These results are in good agreement with the morphological description performed in the field (Table 1). Fine and medium platy and granular structures dominated the Ap horizon. Consequently, the scanner detected many SSGs (Fig. 7, SSG density, SSG fraction, relative surface area) outlining small units (Fig. 7, average unit size). Disagreement between structure size described in the field and the large average unit size (from digital data analysis) in the Bt1 horizon may be explained by several factors. The morphological description was completed shortly after exposing the soil profile but MLT scan data was not collected until 36 hours after exposure. Higher moisture content at the time of description obscured the expression of some structural units. Separation of these units became more prominent as the profile dried before scanning due to their shrinking associated with drying. Some units visible in the resulting data were incompletely or discontinuously outlined by SSGs. This increased average unit sizes since those units consisted of multiple individual structures. The A horizon, for example, had an average unit size of 73 mm, which was slightly larger than the width of coarse plus medium blocky structures. These were the most common structure sizes and types described in the horizon. It is also possible that structure sizes described in the field did not adhere strictly to the assigned size classes. Despite these possible error sources, average unit size for the lower three horizons (24, 31, and 25 mm, respectively) correspond closely with the most common sizes described in the field (Table 1).

We found a strong relationship between SSG size and shape since large SSGs ($A^{1/2}$ > 2 mm) were also predominantly elongated (circularity < 0.5). The relative frequencies of the orientations of these SSGs (Fig. 8) correspond roughly with structure type from the morphological description (Table 1). The 0-8 cm depth, where platy and granular structures were described, shows the majority of SSGs in horizontal or near-horizontal orientations. Descriptions of wedge structure in the 2Btss2 and 2Btss3 horizons are reflected by the relative abundance of SSGs oriented vertically and at approximately 60° left or right of vertical. Agreement between qualitative description of structural morphology and quantitative structural metrics may be affected by the nature of MLT scanning. As the vertical laser stripes move from right to left across the surface, vertical SSGs may be easier for the scanner to capture although we did not examine this effect directly. Analysis of SSG orientation is also complicated in cases where SSGs have both vertical and horizontal units (e.g., L-shaped pores), producing best-fit ellipses oriented diagonally. This effect may have some influence on results for the Btss1 horizon. The strong vertical unit for SSGs in the Bt1 and Bt2 horizons can be largely explained by the lower total quantity of visible SSGs and the prominence of vertical SSGs in those horizons. Future work is needed to refine the characterization of SSG orientation, especially for complex SSG geometries comprised of one or more sections positioned both vertically and horizontally. Segmentation of such SSGs may produce a more accurate characterization of structure, though it would be essential to account for the connectivity of individual segments. It may also be beneficial to further divide SSG orientation by size or by functional characteristics (Greenland and Pereira, 1977; Luxmoore, 1981).

We compared SSG metrics by structure type as described in the field (Fig. 9). SSG fraction and relative surface area show a distinct increase for wedge structure over horizons

where blocky structure was described, which indicate larger average unit sizes. Fewer and generally larger structures were observed in the A and Bt1 horizons (blocky structure) than the 2Btss2 and 2Btss3 horizons where wedge structures were observed. The relatively high values for SSG density, SSG fraction, and relative surface area of the platy/granular category reflect the somewhat looser packing arrangement of these structures in the Ap horizon. These results generally reflect the conditions described in the field.

CONCLUSIONS

This study describes and offers solutions for several practical challenges with MLT scanning of excavation walls in the field. Results show that merging individual scans is unnecessary and may actually decrease accuracy. Data from directly in front of the scanner should either be supplemented with data from an overlapping scan, or cropped out of the AOI before analysis. Here, we used data taken from the left side of the pit along with the overlapping area from right side scan of at least 10 cm. Data taken from the right side that did not overlap was cropped out to eliminate inaccuracies associated with the scanner view angle.

The kind of high-resolution, quantitative data captured by MLT scanning holds great potential for studies of soil genesis and hydropedology, as well as modeling hydrologic processes. Size and shape metrics for both SSGs and digital profile units (representing soil structural units) can be combined with parameters characterizing SSG orientation to produce a quantitative description of soil structure. Measuring soil structure as a continuous variable rather than assigning categorical quantification also allows more subtle differences to emerge that are either inconspicuous or simply disregarded during morphological description or when defining structure categorically.

REFERENCES

Abate, D., R. Ciavarella, G. Furini, G. Guarnieri, S. Migliori, and S. Pierattini. 2011. 3D modeling and remote rendering technique of a high definition cultural heritage artefact. Procedia Computer Science 3:848-852.

Abbasinejad, F., Y.J. Kil, A. Sharf, and N. Amenta. 2009. Rotating scans for systematic error removal. p. 1319-1326. *In* M. Alexa and M. Kazhdan (eds.) Proc. Eurographics Symposium on Geometry Processing. Vol. 28. Berlin, Germany. 15-17 July 2009. Blackwell Publishing, Oxford, UK.

Abou Najm, M.R., J.D. Jabro, W.M. Iversen, R.H. Mohtar, and R.G. Evans. 2010. New method for the characterization of three-dimensional preferential flow paths in the field. Water Resources Research 46:W02503.

Adams, T.L., C. Strganac, M.J. Polcyn, and L.L. Jacobs. 2010. High resolution three-dimensional laser-scanning of the type specimen of Eubrontes (?) Glenrosensis Shuler, 1935, from the Comanchean (Lower Cretaceous) of Texas: Implications for digital archiving and preservation. Palaeontologia Electronica 13:1-11.

Allaire, S.E., S. Roulier, and A.J. Cessna. 2009. Quantifying preferential flow in soils: A review of different techniques. Journal of Hydrology 378:179-204.

Asahina, D., and M.A. Taylor. 2011. Geometry of irregular particles: Direct surface measurements by 3-d laser scanner. Powder Technology 213:70-78.

Barney, A., S. Martelli, A. Serrurier, and J. Steele. 2012. Articulatory capacity of Neanderthals, a very recent and human-like fossil hominin. Philosophical Transactions of The Royal Society of London B: Biological Sciences 367:88-102.

Batey, T. 2000. Soil profile description and evaluation. p. 595–628. *In* K. A. Smith and C. E. Mullins (eds.) Soil and environmental analysis: Physical methods. 2nd ed. Books in Soils, Plants, and the Environment. Marcel Dekker Inc., New York.

Clarkson, C., and P. Hiscock. 2011. Estimating original flake mass from 3d scans of platform area. Journal of Archaeological Science 38:1062-1068.

DeSilva, J.M. 2009. Functional morphology of the ankle and the likelihood of climbing in early hominins. Proceedings of the National Academy of Sciences 106:6567-6572.

DeSilva, J.M. 2010. Revisiting the "midtarsal break". American Journal of Physical Anthropology 141:245-258.

Engleman, E.E., L.L. Jackson, and D.R. Norton. 1985. Determination of carbonate carbon in geological materials by coulometric titration. Chemical Geology 53:125-128.

Gee, G.W., and D. Or. 2002. Particle-size analysis. p. 255-293. *In* J. H. Dane and G. C. Topp (eds.) Methods of soil analyses. Part 4. Physical methods. Ser. No. 5. Soil Science Society of America, Inc., Madison, Wisconsin.

Greenland, D.J., and H.C. Pereira. 1977. Soil damage by intensive arable cultivation: Temporary or permanent? [and discussion]. Philosophical Transactions of the Royal Society B: Biological Sciences 281:193-208.

Grossman, R.B., and T.G. Reinsch. 2002. Bulk density and linear extensibility. p. 201-228. *In* J. H. Dane and G. C. Topp (eds.) Methods of soil analyses. Part 4. Physical methods. Ser. No. 5. Soil Science Society of America, Inc., Madison, Wisconsin.

Guidi, G., F. Remondino, G. Morlando, A. Del Mastio, F. Uccheddu, and A. Pelagotti. 2007. Performance evaluation of a low cost active sensor for cultural heritage documentation. p. 59-69. *In* A. Gruen and H. Kahmen (eds.) Proc. VIII Conference on Optical 3D

Measurement Techniques. Vol. 2. Zurich, Switzerland. 9-12 July 2007. Swiss Federal Institute of Technology, Zurich.

Harden, J. 1982. A quantitative index of soil development from field descriptions: Examples from a chronosequence in central California. Geoderma 28:1-28.

Hillel, D. 1998. Environmental soil physics. Academic Press, New York.

Hirmas, D.R. 2013. A simple method for removing artifacts from moist fine-textured soil faces. Soil Science Society of America Journal. 77:591-593.

Jackson, L.L., and S.R. Roof. 1992. Determination of the forms of carbon in geologic materials. Geostandards Newsletter 16:317-323.

Kettle, W.D., P.M. Rich, K. Kindscher, G.L. Pittman, and P. Fu. 2000. Land-use history in ecosystem restoration: A 40-year study in the prairie-forest ecotone. Restoration Ecology 8:307-317.

Knighton, M.S., D.S. Agabra, W.D. McKinley, J.Z. Zheng, D.D. Drobnis, J.D. Logan, B.F. Bahhour, J.E. Haynie, K.H. Vuong, A. Tandon, K.E. Sidney, and P.L. Diaconescu. 2005. Three dimensional digitizer using multiple methods. U.S. Patent US 6,980,302 B2 2005.

Lepore, B.J., C.L.S. Morgan, J.M. Norman, and C.C. Molling. 2009. A mesopore and matrix infiltration model based on soil structure. Geoderma 152:301-313.

Lin, H. 2010. Linking principles of soil formation and flow regimes. Journal of Hydrology 393:3-19.

Logan, M. 2010. Biostatistical design and analysis using R: A practical guide. Wiley-Blackwell, Singapore.

Luxmoore, R.J. 1981. Microporosity, mesoporosity, and macroporosity of soil. Soil Science Society of America Journal 45:671-672.

McKenzie, D.C. 2001. Rapid assessment of soil compaction damage. 1. The SOILpak score, a semi-quantitative measure of soil structural form. Australian Journal of Soil Research 39:117-125.

McKenzie, N. 2006. A pedologist's view on the future of soil science. p. 89-91. *In* A. E. Hartemink (ed.) The future of soil science. International Union of Soil Sciences, Wageningen, The Netherlands.

Peerlkamp, P.K. 1967. Visual estimation of soil structure. p. 216-223. *In* M. de Boodt, et al. (eds.) West European methods for soil structure determination. Ser. 11. State Faculty Agricultural Sciences, Ghent, Belgium.

Platt, B.F., S.T. Hasiotis, and D.R. Hirmas. 2010. Use of low-cost multistripe laser triangulation (MLT) scanning technology for three-dimensional, quantitative paleoichnological and neoichnological studies. Journal of Sedimentary Research 80:590-610.

Polo, M.E., and A.M. Felicisimo. 2012. Analysis of uncertainty and repeatability of a low-cost 3D laser scanner. Sensors (Basel) 12:9046-9054.

Rossi, A.M., and R.C. Graham. 2010. Weathering and porosity formation in subsoil granitic clasts, Bishop Creek moraines, California. Soil Science Society of America Journal 74:172.

Rossi, A.M., D.R. Hirmas, R.C. Graham, and P.D. Sternberg. 2008. Bulk density determination by automated three-dimensional laser scanning. Soil Science Society of America Journal 72:1591-1593.

Schoeneberger, P.J., D.A. Wysocki, E.C. Benham, and W.D. Broderson. 2002. Field book for describing and sampling soils, ver. 2.0. NRCS, NSSC, Lincoln, Nebraska.

Sholts, S.B., L. Flores, P.L. Walker, and S.K.T.S. Wärmländer. 2011. Comparison of coordinate measurement precision of different landmark types on human crania using a 3D laser scanner and a 3D digitiser: Implications for applications of digital morphometrics. International Journal of Osteoarchaeology 21:535-543.

Sholts, S.B., D.J. Stanford, L.M. Flores, and S.K.T.S. Wärmländer. 2012. Flake scar patterns of Clovis points analyzed with a new digital morphometrics approach: Evidence for direct transmission of technological knowledge across early North America. Journal of Archaeological Science 39:3018-3026.

Sholts, S.B., S.K.T.S. Wärmländer, L.M. Flores, K.W. Miller, and P.L. Walker. 2010. Variation in the measurement of cranial volume and surface area using 3D laser scanning technology. Journal of Forensic Sciences 55:871-876.

Soil Survey Staff. 2012. Web soil survey. Natural Resources Conservation Service, US Department of Agriculture. Available at http://websoilsurvey.nrcs.usda.gov/ (accessed 9 Nov.)

Wright, D.F., and P.A. Selden. 2011. A trigonotarbid arachnid from the Pennsylvanian of Kansas. Journal of Paleontology 85:871-876.

Table 1. Selected morphological, physical, and chemical properties of the soil profile examined in this study.†

Horizon	Depth	Boundary‡	Moist Color	Structure§		PSD¶			Texture#	ρ_b††	OC‡‡
				Description	Size Range	Sand	Silt	Clay			
	cm				mm		%			g cm^{-3}	%
Ap	0-8	cs	10YR 3/1	1mpl,1f,2mgr	1-5	5.1	72.6	22.3	sil	1.06±0.01	2.82
A	8-22	vw	10YR 3/1	3m,cosbk,2f,mabk	5-50	4.6	70.7	24.7	sil	1.31±0.03	1.59
Bt1	22-39	cw	10YR 4/3	3vf,1m,cosbk,3vfabk	0-50	4.8	65.3	29.9	sicl	1.30±0.05	0.94
Bt2	39-54	cw	10YR 4/3	1f,mpr/2f,mabk	5-50	4.8	59.1	36.1	sicl	1.43±0.03	0.62
Btss1	54-61	aw	10YR 4/4	1f pr/2vf,fabk	0-20	3.5	46.9	49.6	sic	1.44±0.01	0.38
2Btss2	61-85	cw	10YR 5/3	3vf,f,m,2coweg	0-100	3.0	43.1	53.9	sic	1.35±0.08	0.31
2Btss3	85-108		10YR 5/4	2vf,f,mweg	0-50	3.1	39.6	57.3	sic	1.31±0.02	0.18

† Bulk density values are followed by ± 1 standard deviation.

‡ c, clear; s, smooth; v, very abrupt; w, wavy; a, abrupt.

§ 1, weak; 2, moderate; 3, strong; vf, very fine; f, fine; m, medium; co, coarse; pl, platy; gr, granular;

¶ PSD, particle-size distribution.

sil, silt loam; sicl, silty clay loam; sic, silty clay.

†† ρb, bulk density.

‡‡ OC, organic carbon.

Table 2. Description of directly measured metrics of SSG size and shape and formulas for composite metrics.

Metric	Variable	Formula	Notes
		SSG Size Metrics	
Area (mm^2)	A		May be expressed as $A^{1/2}$ (mm) representing the side length of a square with equivalent area
Perimeter (mm)	P		May be expressed as P / 4 (mm) representing the side length of a square with equivalent perimeter
Bounding Box Width (mm)	W		Box drawn parallel to x and y axes; Origin in upper left corner, so width may exceed height
Bounding Box Height (mm)	H		Box drawn parallel to x and y axes; Origin in upper left corner, so width may exceed height
Major Ellipse Axis (mm)	E_{maj}		Equivalent area, same orientation and centroid as pores for which ellipse is drawn
Minor Ellipse Axis (mm)	E_{min}		Equivalent area, same orientation and centroid as pores for which ellipse is drawn
Feret Diameter (mm)	F		Maximum caliper distance (i.e., longest distance between parallel tangents to the SSG)
Minimum Feret Diameter (mm)	F_{min}		Minimum caliper distance
		SSG Shape Metrics	
Major Ellipse Axis Angle (°)	L_{maj}		Measured counterclockwise from x-axis or a parallel; $-90° < L_{maj} < 90°$ where 0° is vertical
Minor Ellipse Axis Angle (°)	L_{min}		Measured counterclockwise from x-axis or a parallel; $-90° < L_{maj} < 90°$ where 0° is vertical
Circularity	C	$4\pi (A / P^2)$	Unitless; Range 0-1; C = 1 for a perfect circle and decreases as shape becomes less circular
Roundness	R	$4A / (\pi E_{maj}^2)$	Unitless
Aspect Ratio	M	E_{maj} / E_{min}	Unitless
		Composite Metrics	
Cross-sectional Area (mm^2)	A_{xs}†		For each horizon or area of interest; Used to calculate SSG density, fraction, relative surface area, and average unit size
Number of SSGs	N		Count
Total SSG Area (mm^2)	A_{SSG}	$\sum_{i=1}^{N} A_i$	
Total SSG Perimeter (mm)	P_{SSG}	$\sum_{i=1}^{N} P_i$	
SSG Density (no. / mm^2)	ρ_{SSG}	N / A_{xs}	
SSG Fraction	X	A_{SSG} / A_{xs}	Unitless
Relative SSG Surface Area (mm^{-1})	A_{rel}	P_{SSG} / A_{xs}	
Average Unit Size (mm)	S	$[(A_{xs} - A_{SSG})*4] / P_{SSG}$	Units (i.e., soil aggregates and peds) are outlined by SSGs

† Subscript 'xs' refers to cross section.

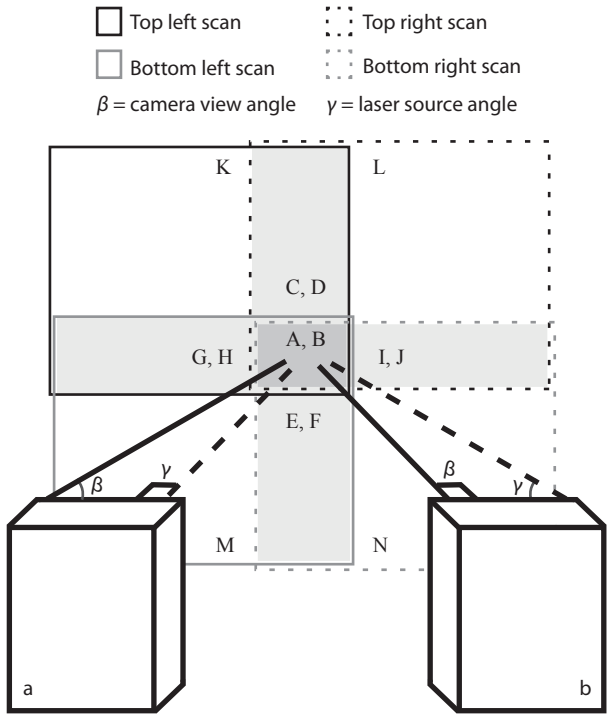

Fig. 1. Four individual scans (L-N) produced 14 unique overlap configurations: all four scans stacked and merged (A, B), both top scans stacked and merged (C, D), both bottom scans stacked and merged (E, F), both left scans stacked and merged (G, H), both right scans stacked and merged (I, J), and each individual scan - top left (K), top right (L), bottom left (M), bottom right (N). The overlap test was conducted only in the central overlap area (dark gray) common to all scans. Camera angle and laser source angle vary as scanner position is adjusted to capture different areas of the excavation wall, as demonstrated by bottom left (a) and bottom right (b) scan positions. The effects of shading caused by irregularities on the excavation wall vary as β and γ change with scanner position.

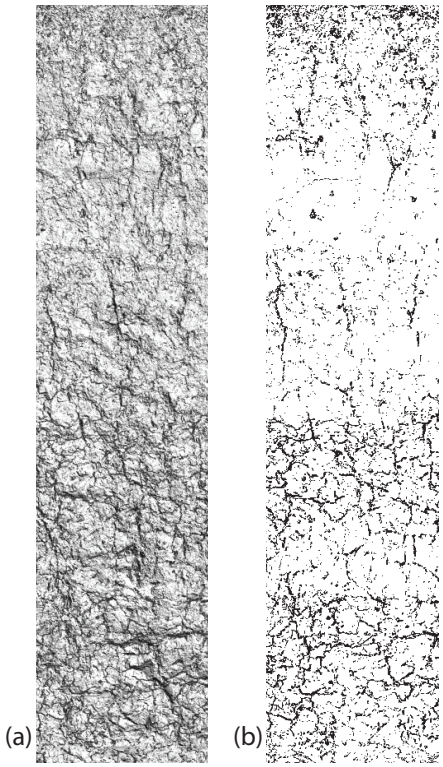

Fig. 2. Complete digital profile shown (a) as exported from ScanStudio HD, and (b) binarized and inverted in ImageJ with surface scan gaps (SSGs) in black.

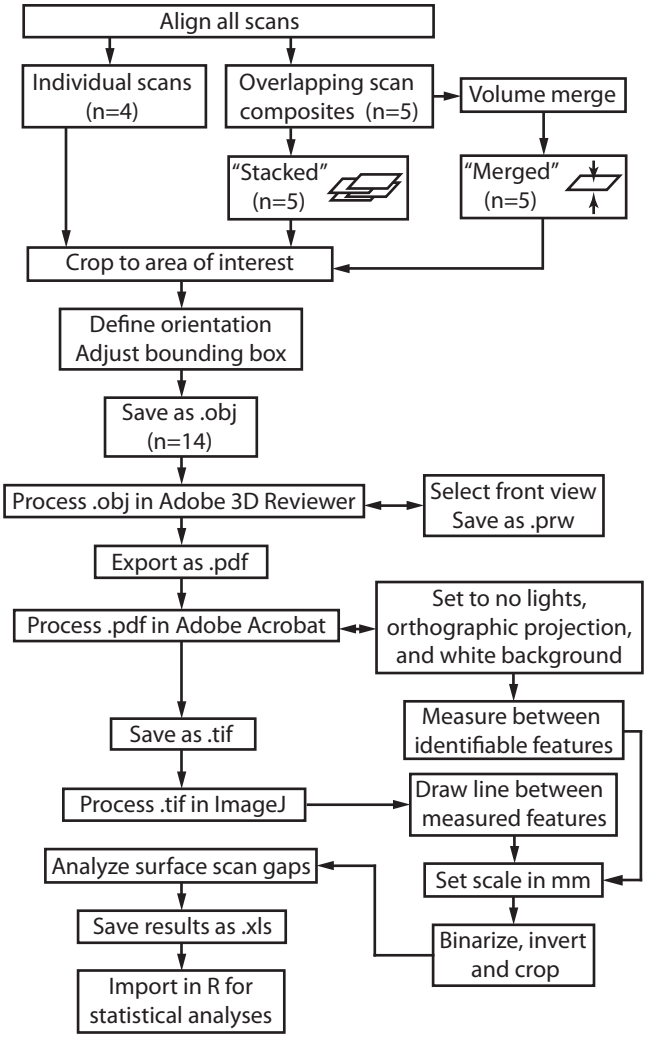

Fig. 3. Flowchart outlining post-processing procedures followed for the overlap test.

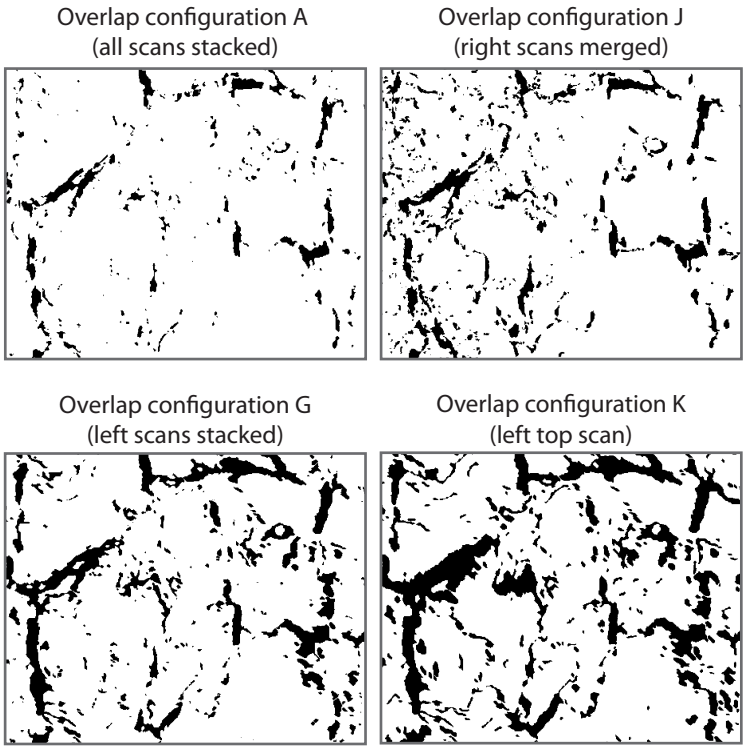

Fig. 4. Select data configurations (binarized, with surface scan gaps in black) from the overlap test. Each image covers the same 94 mm (width) x 76 mm (height) area within the 2Btss2 horizon.

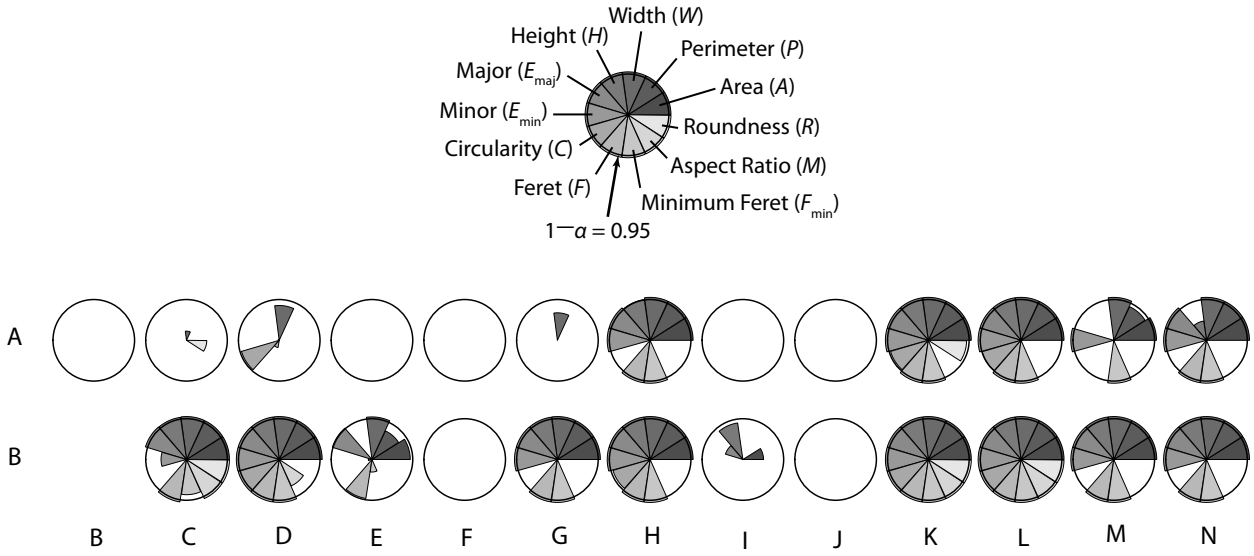

Fig. 5. Star plots displaying 1−*P* values from 11 parameters (abbreviations in Table 2) in 14 overlap configurations: all scans stacked (A) and merged (B); top scans stacked (C) and merged (D); bottom scans stacked (E) and merged (F); left scans stacked (G) and merged (H); right scans stacked (I) and merged (J); left top (K); right top (L); left bottom (M); right bottom (N). Slices extending to rings or beyond indicate a significant difference between overlap treatments for that variable. Familywise error rate accounted for by the Bonferroni method.

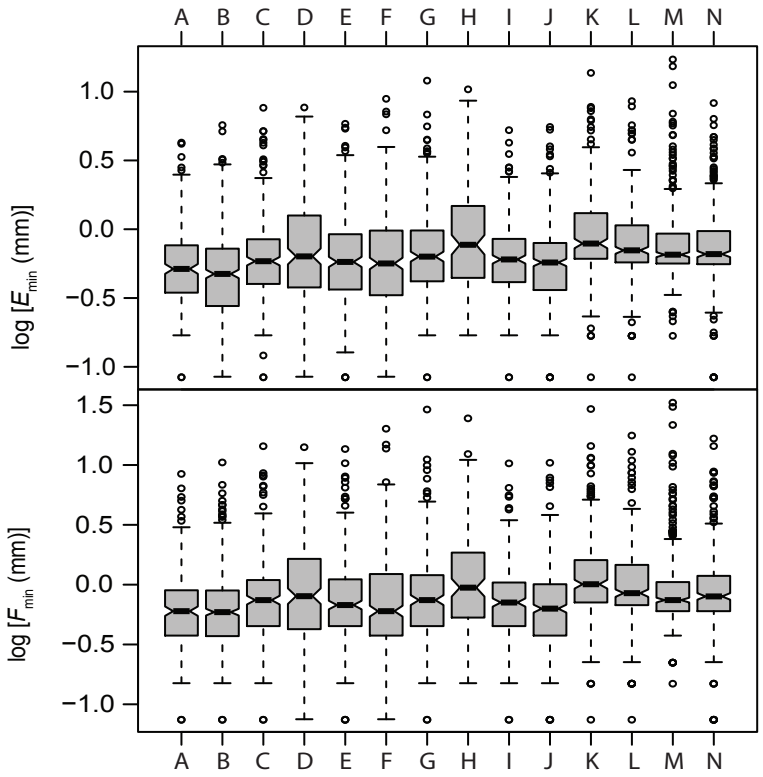

Fig. 6. Boxplots of selected variables (E_{min}, minor ellipse axis; F_{min}, minimum feret diameter) for all 14 overlap configurations: all scans stacked (A) and merged (B); top scans stacked (C) and merged (D); bottom scans stacked (E) and merged (F); left scans stacked (G) and merged (H); right scans stacked (I) and merged (J); left top (K); right top (L); left bottom (M); right bottom (N). Boxes show the upper and lower quartiles, center bars show median values, whiskers extend to extreme data points (with a distance from the box of no more than 1.5 times the interquartile range), points show very extreme values, and notches around center bars are roughly 95% confidence intervals around the median values.

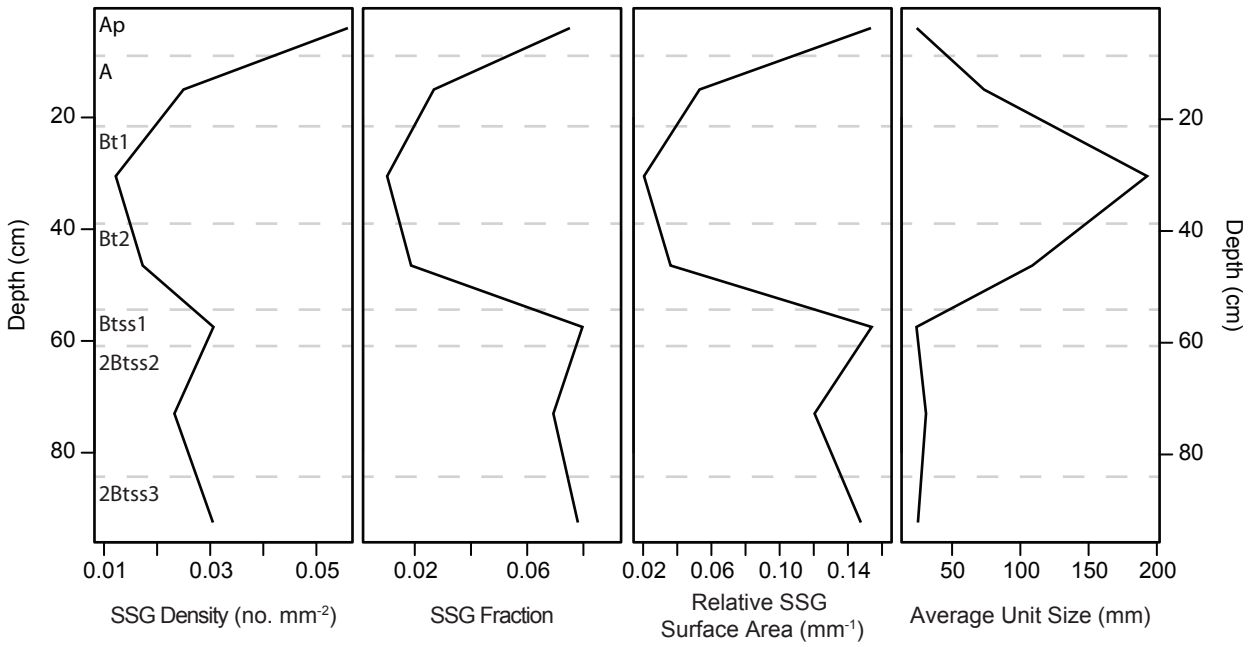

Fig. 7. Composite measurements plotted by horizon. Horizons (separated by gray lines) are labeled in surface scan gap (SSG) density plot.

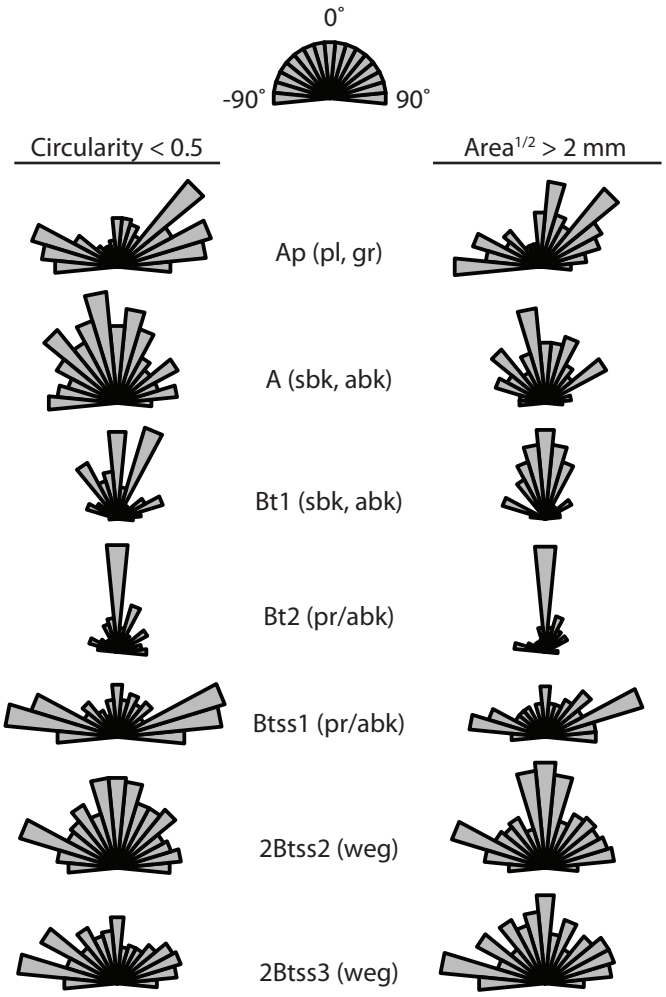

Fig. 8. Angle of major ellipse axis by horizon for all surface scan gaps (SSGs) with Circularity < 0.5 (left), and angle of major ellipse axis for SSGs with Area$^{1/2}$ > 2 mm (right). Horizon names are listed in the center column with corresponding structure types in parentheses, with '/' symbolizing 'parting to'.

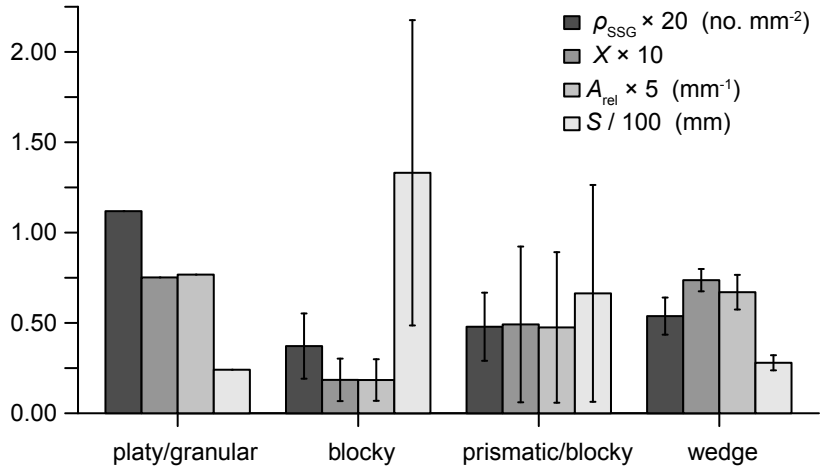

Fig. 9. Mean values by structure type for surface scan gaps (SSGs) with Area$^{1/2}$ > 2 mm. Corresponding horizons are: Ap (platy-granular); A and Bt1 (blocky); Bt2 and Btss1 (prismatic/blocky); 2Btss2 and 2Btss3 (wedge). Error bars represent standard deviation around mean values. Standard deviation not displayed for platy/granular since that structure type was observed in only one horizon.

CHAPTER 3. RELATING QUANTITATIVE SOIL STRUCTURE METRICS TO HYDRAULIC PROPERTIES

ABSTRACT

Soil water flux impacts a range of important soil and environmental processes and is controlled, in part, by soil structure, which may create highly conductive pores that preferentially transmit soil water. Water flux can be modeled when hydraulic properties of the material, such as saturated hydraulic conductivity (K_s) and water retention curve (WRC) parameters, are known. However, K_s and the WRC parameters are strongly tied to soil structure, which is difficult to quantitatively characterize. In this study, we explore relationships between soil hydraulic parameters and quantitative characterizations of soil structure obtained from multistripe laser triangulation (MLT) scanning. A lysimeter (25.4 cm inside diameter x 63.5 cm length) was installed in a Grundy soil series near a MLT-scanned soil profile and adjacent Ameriflux eddy covariance station. Sensors to measure soil water content and temperature were installed at depths of 5, 12.5, 35, and 55 cm within the lysimeter. Software HYDRUS 1-D was used to inversely model K_s and WRC parameters using measurements of soil water content during a 10-day period in April 2013. Results were then validated by a forward solution with data from a 2-day period in April 2012. We identified correlations between parameters defining the water retention curve and both normalized average unit size and standard deviation of the minor ellipse-axis length. A strong positive relationship was also found between K_s and normalized average surface scan gap (SSG) size. Analysis of the coefficient of determination (r^2) across a range of soil water potentials (h) revealed that this relationship is strongest at h = -9.2 cm. Quantitative characterizations of soil structure obtained through MLT scanning

show strong relationships to soil water hydraulic parameters. These relationships hold promise for informing water flux models by parameterizing soil structure as a continuous variable using field-based soil measurements.

INTRODUCTION

Soil water flux affects many important soil and environmental processes including root water uptake, nutrient and contaminant transport, and aquifer recharge. The flux of water into and through soil can often be modeled if the hydraulic properties of the material are known (e.g., Lambot et al., 2002). The specific hydraulic properties needed depend on the model being used to simulate water flux but most often include saturated hydraulic conductivity (K_s) and parameters describing the water retention curve (WRC).

The aggregation of soil particles, which gives rise to soil structure, creates highly conductive interaggregate pores that serve as preferential conduits for the transmission of soil water significantly altering soil hydraulic properties (e.g., Lin et al., 1999; Kutílek, 2004). The presence and morphology of soil structure and concomitant pore networks, however, have been difficult to describe quantitatively. Given the strong dependence of K_s and the WRC parameters on soil structure, they are also difficult to accurately predict at scales influenced by soil structure and relevant to soil water flux in the field (i.e., decimeters to meters). Although the importance of K_s for many soil processes and applications is widely known, and it is used in many calculations and models, K_s is a scale-dependent and time-consuming property to measure. This is unfortunate because accurate modeling of soil water flux depends, in part, on accurate quantitative parameterizations of the soil water flux pathways (Vanclooster et al., 2005).

Recent work has shown that a novel structured-light scanning technique—known as multistripte laser triangulation (MLT)—has the ability to quantify soil structure for an entire soil profile by capturing the geometric information of interpedal pore spaces in the field (Eck et al., 2013). With MLT, a laser scanner monitors the apparent deformation of parallel vertical laser stripes as they sweep across a surface and computes distances by detecting variations in light intensity of the projected laser stripes (Knighton et al., 2005; Platt et al., 2010). The resulting digital data is a triangulated irregular network with areas of missing data where no return was detected by the scanner. Eck et al. (2013) termed these areas of missing data 'scan surface gaps' (SSGs) and assumed that they represent preferential flow paths (PFPs) in the soil. By characterizing and quantifying PFPs, MLT scanning opens up the potential for directly examining the relationship between soil structure and hydraulic properties. The primary objective of this work was to investigate the relationships between MLT-derived SSG metrics and both K_s and the parameters of the van Genuchten (1980) water retention function.

MATERIALS AND METHODS

Study Site

This study was conducted in eastern Kansas at the site described in detail by Eck et al. (2013). Briefly, the site is located on an upland topographic position in a tallgrass prairie and oak-hickory forest ecotone (Kettle et al., 2000) which has an average annual temperature of 13.3°C and receives an average of 937 mm of annual precipitation (Brunsell et al., 2013). The soil is mapped as a Grundy silty clay loam (fine, smectitic, mesic, Oxyaquic Vertic Argiudoll; Soil Survey Staff, 2014) in the Nelson Environmental Study Area at the University of Kansas

Field Station in Jefferson County, Kansas. Native grasses such as big and little bluestem, Indian grass, and switch grass cover most of the site (D. Kettle, personal communication, 2012).

Field Lysimeter Installation and Sampling

An annular space was excavated at the site to a depth of 1 m around a column of undisturbed soil. The column was carefully hand-carved to fit tightly into a 25.4-cm i.d. × 63.5-cm length stainless steel ring, which served as the divergence control tube for a passive capillary lysimeter (Drain Gauge G3, Decagon Devices, Inc., Pullman, WA). After reaching a depth of 75 cm, the undisturbed column was removed and a PVC drainage reservoir was installed beneath the original column location. The undisturbed column was repositioned on top of the drainage reservoir with a layer of diatomaceous earth between the soil column and lysimeter wick to provide a good contact surface. Four soil moisture and temperature sensors (5TM, Decagon Devices, Inc., Pullman, WA) were installed in the undisturbed column at depths of 5, 12.5, 35, and 55 cm within the lysimeter. An additional sensor was installed at 100 cm in the outer annular wall approximately 1 m from the lysimeter installation. Soil moisture and temperature measurements were recorded on a data logger (Em50, Decagon Devices, Inc., Pullman, WA) every 30 minutes. A suite of atmospheric variables, including air temperature, air pressure, solar radiation, and precipitation were also monitored by an Ameriflux eddy covariance station directly adjacent to the lysimeter installation.

MLT data collected by Eck et al. (2013) was also used for this investigation. In that study, the soil pit was extended to expose a 1-m profile and was described following Schoeneberger et al. (2002). Briefly, root quantity class was assessed as few, common, or many if the soil contained on average less than 1, between 1 and 5, or greater than or equal to 5 roots

per cm^2 for very fine (<1 mm) and fine (1 to <2 mm) roots. Artifacts produced during excavation of the profile were removed using a freeze method (Hirmas, 2013) and the profile was allowed to dry for 36 h to enhance the visible appearance of soil structure (Eck et al., 2013). An MLT scanner (NextEngine Desktop 3D Scanner Model 2020i, NextEngine Inc., Santa Monica, CA) was used to collect digital data from the profile surface as detailed by Eck et al. (2013). Triplicate bulk density samples were collected from each horizon using 3 × 5.4-cm (inside diameter) brass rings (SoilMoisture Equipment Corp, Santa Barbara, CA). Bulk samples and 3 soil clods were also collected for each horizon to analyze particle-size distribution, organic carbon content, WRC, and coefficient of linear extensibility (COLE). In addition to these samples, we extracted a 6.35-cm diameter soil core using a hydraulic coring machine (Giddings Machine Company, Inc., Windsor, CO) approximately 3 m from the scanned profile. This core was used in a dye study described below to visually examine the relationship between saturated water flux and soil structure.

Laboratory Analyses

The pipette method (Gee and Or, 2002) was used to determine particle-size distribution from the bulk samples after pretreatment to remove organic matter. Bulk density was obtained from the triplicate sampled cores following Grossman and Reinsch (2002). Soil clods and bulk samples were used to measure points along a WRC for each horizon using a hanging column (2 replicates; Brasher et al., 1966), pressure plates (4 replicates; Burt, 2004), and a dewpoint potentiameter (1 replicate; WP4C, Decagon Devices, Inc., Pullman, WA; Leong et al. 2003; ASTM 2003). COLE was also measured for each horizon using the rod method following

Schafer and Singer (1976). Measured values from each WRC were exported to SWRC Fit (Seki, 2007) and fit with the van Genuchten (1980) water retention function:

$$S_e(h) = \frac{\theta - \theta_r}{\theta_s - \theta_r} = \left[1 + (-\alpha h)^n\right]^{-m} \quad [1]$$

where S_e is the effective saturation, θ_s and θ_r are the saturated and residual water contents, respectively, θ is water content at equilibrium with pressure potential h, and α and n are fitting parameters. We used the common simplification that $m = 1–1/n$. Fitted values for the WRC were used as the initial soil hydraulic parameters in HYDRUS 1-D (Šimůnek et al., 2013) to inversely solve the Richards equation for a single porosity model (van Genuchten-Mualem) with no hysteresis and free drainage. The Richards equation can be expressed as:

$$\frac{\partial \theta(h)}{\partial t} = \frac{\partial}{\partial z}\left[K(h)\frac{\partial h}{\partial z}\right] + \frac{\partial K(h)}{\partial z} - S(h) \quad [2]$$

where θ is volumetric water content, h is pressure head, t is time, z is the vertical coordinate, and K is hydraulic conductivity (Radcliffe and Šimůnek, 2010). The hydraulic conductivity function can be expressed as (Radcliffe and Šimůnek, 2010):

$$K(S_e) = K_s S_e^l \left[1 - \left(1 - S_e^{1/(1-1/n)}\right)^{1-1/n}\right]^2 \quad [3]$$

where K is hydraulic conductivity and l is a pore-connectivity parameter.

Initial values for K_s were predicted by a neural network (Rosetta Lite v. 1.1; Schaap et al., 2001) using particle-size distribution and bulk density. An initial value of 0.5 was used for the pore-connectivity parameter, l, for all horizons. Roots were input using a relative scale by considering the abundance of fine and very fine roots described at the site. Medium roots were excluded since roots of these sizes were estimated using a larger assessment window (i.e., 1 dm^2 compared to 1 cm^2). Within each horizon, the abundance of fine and very fine roots were summed and divided by 10 to scale the final root distribution values below 1. The abundance

category of 'many' was assigned a value of 5 cm^{-1}, 'common' was assigned a value of 3 cm^{-1}, and 'few' assigned a value of 1 cm^{-1} corresponding to the lower, middle, and highest value in those categories multiplied by the length of the assessment window, respectively. For example, in the 0-8 cm horizon, we observed many very fine and common fine roots which were converted to a value of 0.8 cm^{-1} [i.e., (5 cm^{-1} + 3 cm^{-1})/10]. Leaf area index was obtained from MODIS satellite data at a 1-km resolution and processed to obtain the value for the pixel containing the study site (Wan, 2008; Wan, 2009).

The model was run inversely for a 10-day period in April of 2013. Soil moisture data for the inverse solution was obtained from the lysimeter; precipitation and potential evapotranspiration data (PET) were taken from eddy covariance tower measurements and used as the time-variable boundary conditions in HYDRUS 1-D. Soil hydraulic parameters were optimized by running the model repeatedly and making incremental adjustments to starting values and parameters to be solved for each solution attempt. After completion of the calibration run, a two-day period of soil moisture, precipitation, and PET observations was chosen from a similar time of the previous year (April, 2012) to validate the hydraulic parameters produced by the inverse calibration solution. Since the validation run covers a relatively short time period, roots were not parameterized in an attempt to shorten the model processing time because they were not expected to heavily impact the results.

As detailed by Eck et al. (2013), data collected from the MLT scans of the soil profile were processed and separated by horizon in ScanStudio HD (NextEngine Inc., Santa Monica, CA) and analyzed in ImageJ (Research Services Branch, National Institute of Health, Bethesda, MD). Scan data was binarized in ImageJ to exclude the solids, leaving only SSGs for analysis. Results of the image analyses were imported into R 3.0.1 (R Development Core Team, Vienna,

Austria) for statistical analysis where composite metrics were calculated for each horizon following Eck et al. (2013). Soil profile metrics were correlated with the optimized K_s to examine the relationship between soil structure and soil hydraulic conductivity.

Quantitative metrics used to characterize the soil profile—shown in Eck et al. (2013)—included normalized average unit size, standard deviation of the best-fit ellipse minor axis length (E_{min}), and normalized average SSG size ($\widetilde{W}$). Average unit size (S) for a given horizon within the soil profile is expressed as:

$$S = \left[\left(A_{xs} - A_{SSG}\right) \cdot 4\right] / P_{SSG} \quad [4]$$

where A_{xs} is the cross-sectional area, A_{SSG} represents the total SSG area, and P_{SSG} is the total SSG perimeter. We then divided S by COLE to normalize the values for each horizon. The next quantitative metric used was the standard deviation of the minor ellipse axis length. Best-fit ellipses are drawn for each SSG in the digital data. The standard deviation of this metric was taken for each horizon as a measurement of the pore-size distribution within each horizon. Normalized average SSG size, $\widetilde{W}$, is calculated using the following equation:

$$\tilde{W} = W^2 \sin\left(L_{maj}\right) / \mathrm{COLE} \quad [5]$$

In this calculation, W is the average width of a bounding box around the SSGs, L_{maj} is the average angle between the major axis of the best-fit ellipse and a horizontal reference.

The 1-m vertical core taken close to the lysimeter was cut into sections by morphological horizon. The top and bottom of each section was cleaned using a freeze method (Hirmas, 2013) to remove any smearing imparted when the core was sliced into sections. The sides of the core sections (i.e., along the length of the core) were tightly wrapped with cellophane and cheesecloth was attached at the bottom to prevent soil loss. A plastic tube was placed just above the top of the core surface inside the cellophane to maintain shape and provide a space for ponding fluid

above the soil. The section was then wrapped with 1.3-cm thick foam padding and tightly bound with hook-and-loop straps to prevent water flow between the soil sample and cellophane wrapping. A segment within the 8-22 cm horizon was saturated by submerging the lower 1 cm in a solution of partially deaerated water, calcium sulfate dihydrate and phenol (modified from Klute and Dirksen, 1986). Methylene blue was ponded on top of the segments and allowed to completely infiltrate in order to highlight PFPs (e.g., Bouma et al., 1977; Hatano and Booltink, 1992; Hangen et al., 2002). The core sections were air dried for approximately 48 h before being split open, photographed, and scanned with an MLT scanner.

RESULTS AND DISCUSSION

Parameter estimations from the HYDRUS 1-D fit are presented in Table 1 and the corresponding WRCs are displayed in Fig. 1. There are 6 hydraulic variables for each horizon but HYDRUS 1-D can only fit up to 15 parameters at once. Initial values for these parameters were obtained from SWRC Fit (Seki, 2007) as mentioned above. Time-variable atmospheric inputs are shown in Fig. 2. Over multiple iterations, various combinations of variables were fixed and others were fitted. Neither θ_r nor θ_s were allowed to vary in any of the model runs. After several iterations, an inverse solution of HYDRUS 1-D produced hydraulic parameters describing WRCs that matched well with WRCs for the measured data (Fig. 1). For the final model run, we used results of previous solutions as initial values, then allowed α, n, and K_s to vary for the top 4 horizons; for the lower 3 horizons, only K_s was allowed to vary. The bottom panel of Fig. 2 shows the predicted soil moisture data are closely aligned with measured values. Since θ_r and θ_s were fixed to the predicted values based on measured water retention data, the resulting WRCs based on the modeled results displayed in Fig. 1 are very closely aligned to

measured data. The exception to the close match between measured and modeled data is found in the 39-54 cm horizon. In the field, we observed primarily weak structure in this horizon, but did note the presence of a few prominent vertical pores. The shape of the curve indicates that water flow within this horizon is largely controlled by large vertical pores. Measured data, however, demonstrate the presence of a range of pore sizes, which can account for the gap between the modeled curve and measured points (Fig. 1). This discrepancy may be explained by the predominance of weak prismatic structure observed in the 39-54 cm horizon. While several vertical PFPs were captured in MLT data, the weak structural expression may have obscured the capture of additional PFPs that were observed in soil profile.

The HYDRUS 1-D model was then run as a forward solution model to validate the hydraulic parameters produced by the inverse solution. This forward run (Fig. 3) verified that hydraulic parameters found by the inverse solution could reasonably describe the observed soil moisture conditions over time. Modeled results for the 100-cm depth exceeded the saturated water content. Since these values were a physical impossibility, we limited those values not to exceed the saturated water content.

Metrics describing SSG size and shape were used to investigate correlations with each of the hydraulic parameters found through the inversion process with HYDRUS 1-D. Normalized average unit size ($\tilde{S}$), standard deviation of $E_{\min}$, and $\widetilde{W}$ were the MLT metrics that showed the strongest relationships with the hydraulic parameters. The α parameter of the van Genuchten (1980) model (Eq. 1), which is related to the air-entry value, was positively correlated with normalized average unit size (Fig. 4). In a soil with lower COLE values, SSGs will be present even at moist conditions. Where COLE values are high, any saturated water flow through soil will be more influenced by matrix flow since SSGs, representing PFPs in the soil profile, will

swell shut. Therefore, smaller structure sizes in soils with vertic properties will have lower α values, and air-entry potential will be higher compared to soils with larger structures. Larger aggregates in soils with lower COLE values can be expected to have higher α values, and therefore, lower air-entry potentials.

The n parameter in Eq. 1 is negatively related to the standard deviation of the minor ellipse axis (E_{min}) length as shown in Fig. 5. This relationship seems to support the notion that broad pore-size distributions or poorly sorted soils (i.e., those with larger standard deviations) tend to have lower values for the n parameter (e.g., van Genuchten, 1980; al Awar, 2008).

Perhaps the most important relationship was found between saturated hydraulic conductivity and $\widetilde{W}$ (Fig. 6). The correction factor of $\sin(L_{maj})$/COLE in Eq. [5] reduces the weight of PFPs as they become more horizontal (i.e., 0°) and also discounts PFPs with higher COLE values, since they would tend to swell shut near saturation.

We regressed the coefficient of determination (r^2) against h in Fig. 7 to ascertain the strength of the relationship between $\widetilde{W}$ and hydraulic conductivity across a range of soil water potentials. While the relationship explains a large amount of the variation in K across the range of pressure heads investigated. The strongest relationship was found at h = -9.2 cm, where r^2 = 0.83. This is indicative of the pore size (163 μm) for which the MLT scanner is best able to characterize PFPs in the soil profile. Even at the pit scale where the scanner is employed for this study, the largest pores in the soil, which exert their largest influence on K as h approaches zero, are not captured in the digital data. There are several possible explanations for such a result. Larger PFPs are often created by biological activity in the soil. Such PFPs may not appear in digital data because the scanner would be able to detect the surfaces of such pathways. In contrast, interpedal PFPs are observed as gaps in the soil fabric and the full extent of the void is

not usually visible in profile. Another possibility is that the largest interpedal PFPs in a given horizon were simply not present in the soil at the given study site.

Finally, the dye study performed on the core sample was visually compared to MLT scan data (Fig. 9) and added further evidence that SSGs in the digital data represent interpedal PFPs observed in the field. Placing a photograph and MLT data side-by-side, several corresponding areas can be clearly recognized. The dye study results demonstrated a close match between areas of dyed soil core sections and SSGs (i.e., missing data) observable in MLT scan data.

CONCLUSIONS

This study illustrates several relationships between quantitative, field-based MLT parameters that characterize soil SSGs and soil hydraulic parameters defining the WRC. The α parameter was positively correlated to the normalized average unit size, and a negative correlation was found between n and the standard deviation of $E_{\min}$. A strong positive relationship was also found between K and $\widetilde{W}$ (normalized average SSG size). MLT scanning is able to obtain quantitative data characterizing SSGs which are related to soil hydraulic parameters, including K_s, for this study site. By quantifying soil structure at the field scale, MLT scanning holds the potential to improve accuracy of K_s values and better quantify heterogeneity within the soil when it can be collected at several points within a given soil type. This ability makes K_s measurements based on observed conditions possible instead of relying on values predicted by pedotransfer functions. It should also improve our ability to parameterize soil structure in water flux models and to quantify it as a continuous variable at the soil pit scale. Future work should investigate additional sites to determine the applicability of the SSG-

hydraulic parameter relationships across multiple soil types and landscape positions found in this study.

REFERENCES

al Awar, Z.R.. 2008. Adapting, optimizing, and evaluating a model for the remediation of LNAPL in heterogeneous soil environments. Doctoral Dissertation, The University of Texas at Austin.

American Society for Testing and Materials (ASTM). 2003. Test methods for determination of the soil water chararcteristic curve for desorption using a hanging column, pressure extractor, chilled mirror hygrometer, and/or centrifuge. ASTM D6836-02, West Conshohocken, Pa.

Bouma, J., A. Jongerius, O. Boersma, A. Jager, and D. Schoonderbeek. 1977. The function of different types of macropores during saturated flow through four swelling soil horizons. Soil Science Society of America Journal 41:945-950.

Brunsell, N.A., J.B. Nippert, and T.L. Buck. 2013. Impacts of seasonality and surface heterogeneity on water-use efficiency in mesic grasslands. Ecohydrology. doi: 10.1002-eco.1455

Decagon Services Ltd. 2002. WP4 User's Manual. Decagon Devices, Inc. Pullman, WA.

Eck, D.V., D.R. Hirmas, and D. Giménez. 2013. Quantifying soil structure from field excavation walls using multistripe laser triangulation scanning. Soil Science Society of America Journal 77:1319-1328.

Gee, G.W., and D. Or. 2002. Particle-size analysis. p. 255-293. *In* J. H. Dane and G. C. Topp (eds.) Methods of soil analyses. Part 4. Physical methods. Ser. No. 5. Soil Science Society of America, Inc., Madison, Wisconsin.

Grossman, R.B., and T.G. Reinsch. 2002. Bulk density and linear extensibility. p. 201-228. *In* J. H. Dane and G. C. Topp (eds.) Methods of soil analyses. Part 4. Physical methods. Ser. No. 5. Soil Science Society of America, Inc., Madison, Wisconsin.

Hangen, E., U. Buczko, O. Bens, J. Brunotte, and R.F. Hüttl. 2002. Infiltration patterns into two soils under conventional and conservation tillage: influence of the spatial distribution of plant root structures and soil animal activity. Soil and Tillage Research 63:181-186.

Hatano, R., and H.W.G. Booltink. 1992. Using fractal dimensions of stained flow patterns in a clay soil to predict bypass flow. Journal of Hydrology 135:121-131.

Hirmas, D.R. 2013. A simple method for removing artifacts from moist fine textured soil faces. Soil Science Society of America Journal 77:591–593. doi:10.2136/sssaj2012.0418n

Kettle, W.D., P.M. Rich, K. Kindscher, G.L. Pittman, and P. Fu. 2000. Land use history in ecosystem restoration: A 40-year study in the prairie-forest ecotone. Restoration Ecology 8:307–317. doi:10.1046/j.1526-100x.2000.80043.x

Klute, A., and C. Dirksen. 1986. Hydraulic conductivity and diffusivity: Laboratory methods. P. 687-734. *In* A. Klute (ed.) Methods of Soil Analysis. Part 1. Physical and Mineralogical Methods. 2nd ed. SSSA Book Series No. 5. SSSA-ASA, Madison, Wisconsin.

Knighton, M.S., D.S. Agabra, W.D. McKinley, J.Z. Zheng, D.D. Drobnis, J.D. Logan, B.F. Bahhour, J.E. Haynie, K.H. Vuong, A. Tandon, K.E. Sidney, and P.L. Diaconescu. 2005. Three dimensional digitizer using multiple methods. U.S. Patent US 6,980,302 B2 2005.

Kutílek, M. 2004. Soil hydraulic properties as related to soil structure. Soil and Tillage Research 79:175-184.

Lambot, S., M. Javaux, F. Hupet, and M. Vanclooster. 2002. A global multilevel coordinate search procedure for estimating the unsaturated soil hydraulic properties. Water Resources Research 38:6-1. doi: 10.1029/2001WR001224

Leong, E. C., S. Tripathy, and H. Rahardjo. 2003. Total suction measurement of unsaturated soils with a device using the chilled-mirror dew-point technique. Geotechnique 53:173-182.

Lin, H.S., K.J. McInnes, L.P. Wilding, and C.T. Hallmaark. 1999. Effects of soil morphology on hydraulic properties I. Quantification of Soil Morphology. Soil Science Society of America Journal. 63:948-954. doi: 10.2136/sssaj1999.634948x

Platt, B.F., S.T. Hasiotis, and D.R. Hirmas. 2010. Use of low-cost multistripe laser triangulation (MLT) scanning technology for three-dimensional,quantitative paleoichnological and neoichnological studies. Journal of Sedimentary Research 80:590–610. doi:10.2110/jsr.2010.059

Radcliffe, D.E. and J. Šimůnek. 2010. Soil physics with HYDRUS: Modeling and applications. CRC Press/Taylor & Francis, Boca Raton.

Schaap, M.G., F.J. Leij, and M. Th. van Genuchten. 2001. Rosetta: a computer program for estimating soil hydraulic parameters with hierarchical pedotransfer functions. Journal of Hydrology 251:163-176.

Schafer, W.M. and M.J. Singer.1976. A new method of measuring shrink-swell potential using soil pastes. Soil Science Society of Amreica Journal 40:805-806. doi: 10.2136/sssaj1976.03615995004000050050x

Schoeneberger, P.J., D.A. Wysocki, E.C. Benham, and W.D. Broderson. 2002. Field book for describing and sampling soils, ver. 2.0. NRCS, NSSC, Lincoln, Nebraska.

Seki, K. 2007. SWRC fit - a nonlinear fitting program with a water retention curve for soils having unimodal and bimodal pore structure. Hydrology and Earth System Sciences Discussions 4: 407-437.

Šimůnek, J., M. Šejna, H. Saito, M. Sakai, and M. Th. van Genuchten, The Hydrus-1D Software Package for Simulating the Movement of Water, Heat, and Multiple Solutes in Variably Saturated Media, Version 4.16, HYDRUS Software Series 3, Department of Environmental Sciences, University of California Riverside, Riverside, California.

Soil Survey Staff. 2014. Web soil survey. Natural Resources Conservation Service, US Department of Agriculture. Available at http://websoilsurvey.nrcs.usda.gov/ (accessed 9 Nov. 2012)

Vanclooster, M., J. Boesten, A. Tiktak, N. Jarvis, J. G. Kroes, R. Munoz-Carpena, B. E. Clothier, and S. R. Green. 2005. On the use of unsaturated flow and transport models in nutrient and pesticide management, p. 331–362. *In* R.A. Feddes, G.H. de Rooij, and J. C. van Dam (eds.) Unsaturated-Zone Modeling: Progress, Challenges and Applications. UR Frontis Ser., Kluwer Academic Publishers, Dordrecht, Netherlands.

van Genuchten, M. 1980. A closed-form equation for predicting the hydraulic conductivity of unsaturated soils. Soil Science Society of America Journal 44:892-898.

Wan, Z.M. 2008. New refinements and validation of the MODIS land-surface temperature/emissivity products. Remote Sensing of Environment, 112:59-74.

Wan, Z.M. 2009. MODIS land surface temperature products users' guide. University of California, Santa Barbara.

Table 1. Hydraulic parameters produced by Hydrus 1-D inverse solution.

Horizon	**Depth**	**COLE†**	**θ_r‡**	**θ_s§**	***α***	***n***	***K_s*¶**	***l*#**
	cm		-------m^3 m^{-3}-------		cm^{-1}		cm d^{-1}	
Ap	0-8	0.054	0.0278	0.537	0.0128	1.81	698	0.22
A	8-22	0.040	0.0366	0.464	0.0121	1.56	722	0.01
Bt1	22-39	0.064	4.1E-08	0.517	0.0199	1.33	64.3	0.01
Bt2	39-54	0.099	4.2E-06	0.524	0.0066	2.17	0.210	0.36
Btss1	54-61	0.121	5.4E-07	0.562	0.0037	1.20	58.3	1.14
2Btss2	61-85	0.116	1.6E-07	0.553	0.0018	1.19	5.82	1.38
2Btss3	85-108	0.142	6.1E-07	0.594	0.0014	1.19	0.280	0.50

†COLE, coefficient of linear extensibility.

‡θ_r, residual water content.

§θ_s, saturated water content.

¶K_s, saturated hydraulic conductivity.

#*l*, pore connectivity parameter.

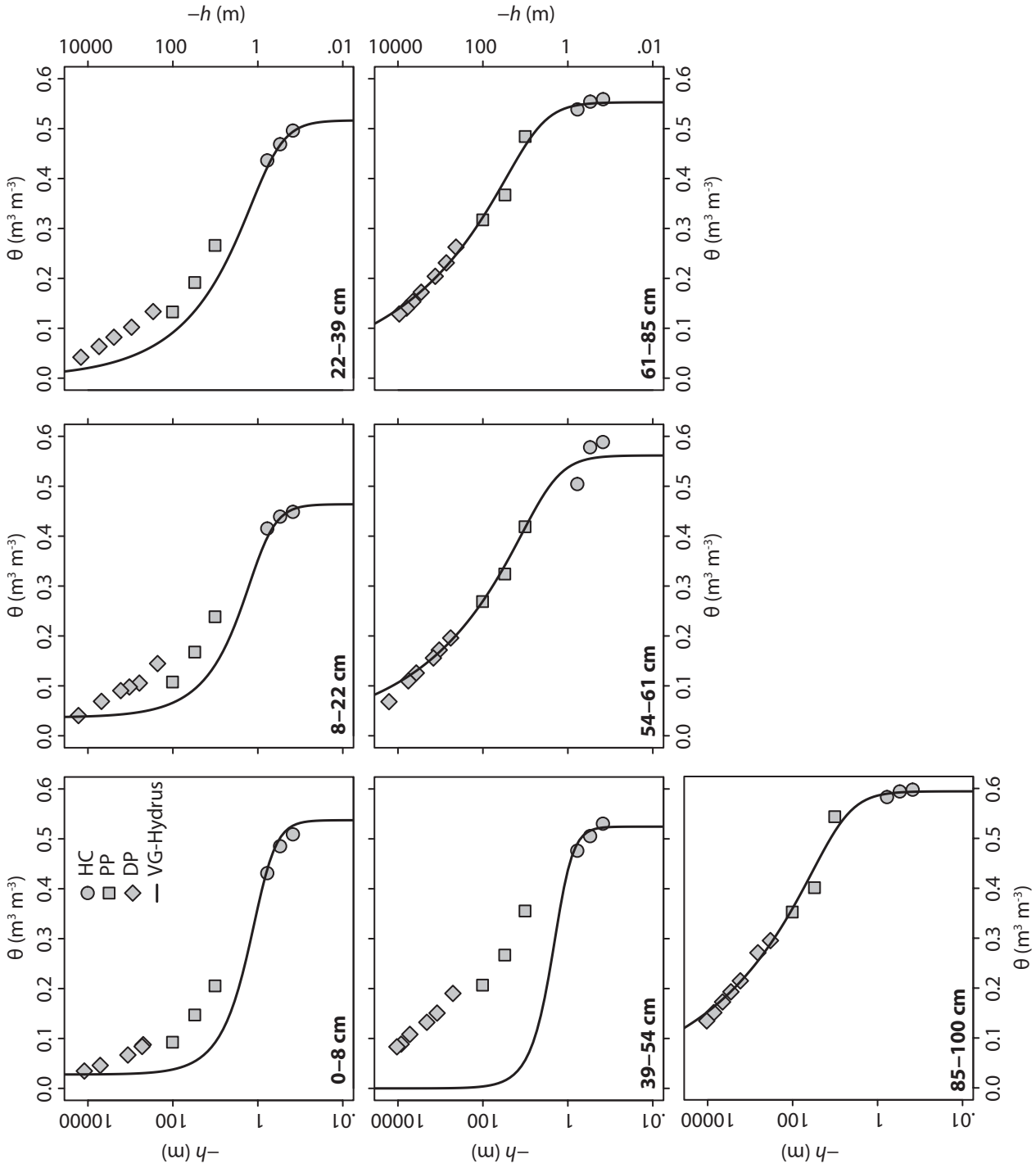

Fig. 1. Water retention curves for all horizons displaying measured data points (HC, hanging column; PP, pressure plate; DP, dewpoint potentiameter) and curves predicted by hydraulic parameters for the van Genuchten (1980) model (VG-Hydrus), which were generated from the Hydrus 1-D calibration fit (i.e., inverse solution). The lower three horizons allowed only K_s to vary while all other hydraulic parameters were fixed during during the calibration.

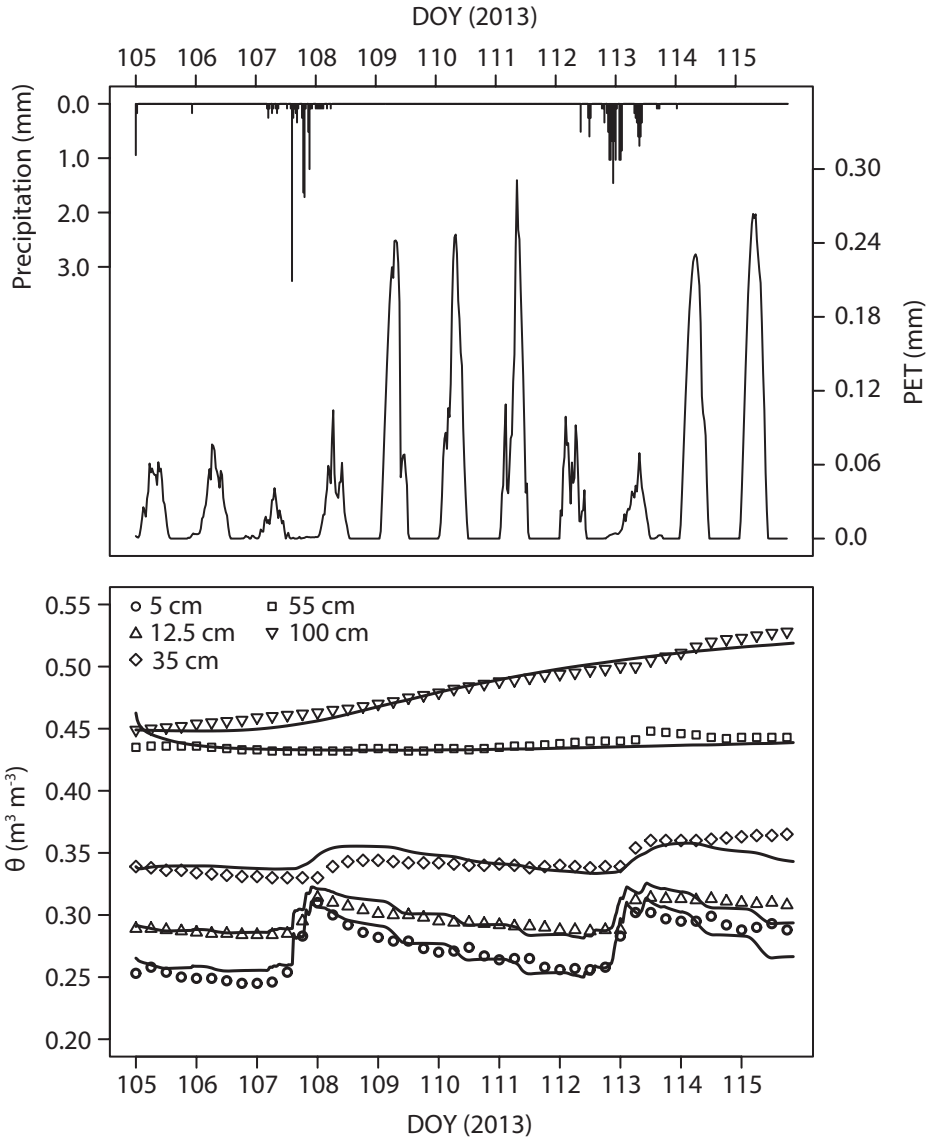

Fig. 2. Plots showing time-variable atmospheric inputs (top) and measured soil moisture data (bottom plot; points) along with Hydus results (bottom plot; lines) at corresponding depths. Measured data points were collected at 30 minute invervals but the plot displays data only every 6 hours for clarity.

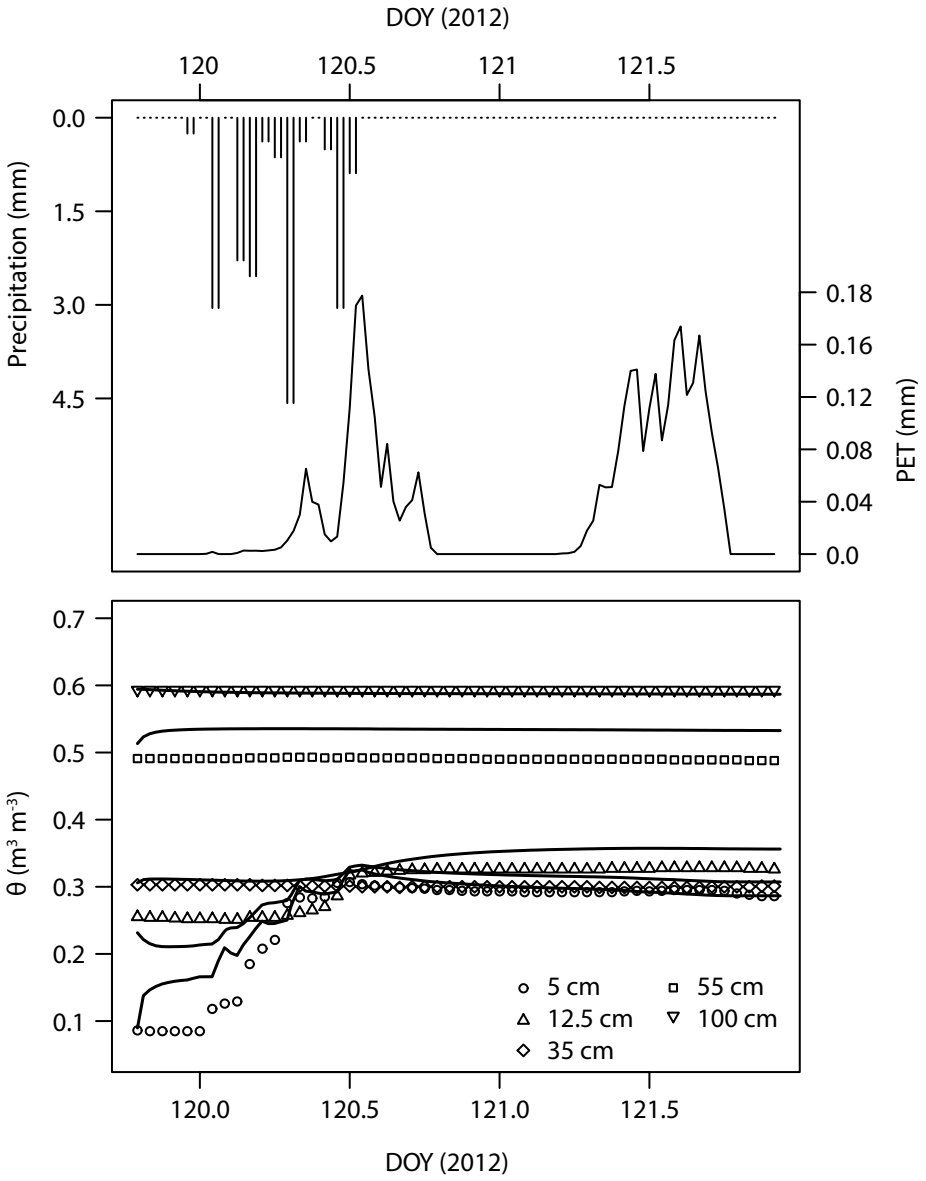

Fig. 3. Input data (precipitation, PET, soil moisture) for Hydrus 1-D validation (i.e., forward prediction) solution. Soil moisture panel (bottom) displays observed soil moisture as points and soil moisture predicted by HYDRUS solution as lines for corresponding depths. Observed soil moisture values for the 100 cm depth exceeded the saturated soil water content and are therefore fixed to the saturated soil water content since the values were not interpretable. Measured data points were collected at 30 minute invervals but the plot displays data only every 2 hours for clarity.

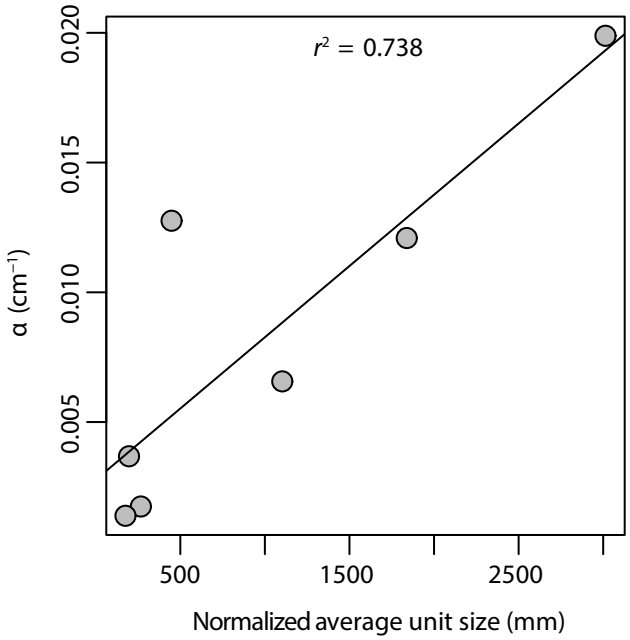

Fig. 4. Average unit size normalized by COLE has a strong positive correlation with the α parameter. Water retention should be lowest when average unit sizes are small and with higher COLE values since air-entry potential is inversely related to α.

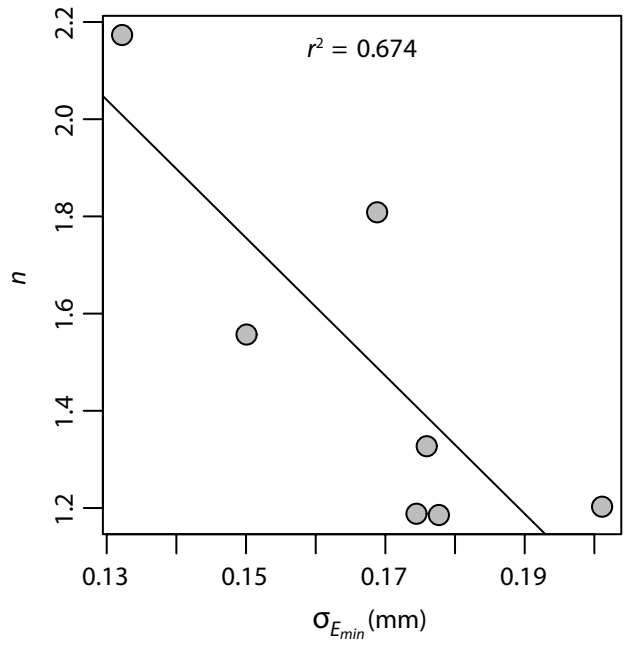

Fig. 5. A negative correlation exists between the hydraulic fitting parameter *n* and standard deviation (σ) of the minor ellipse axis length ($E_{\min}$) for the best-fit ellipse around each pore.

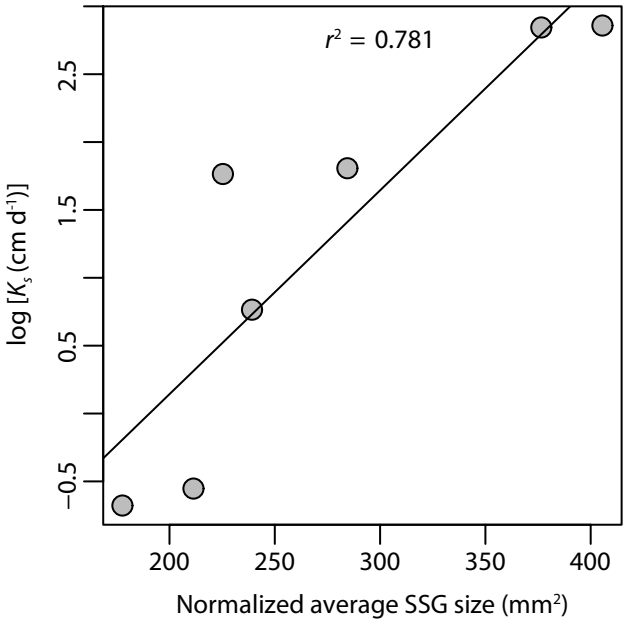

Fig. 6. Saturated hydraulic conductivity as a function of normalized average SSG size. Normalized average SSG size is calculated as $W^2 \sin(L_{maj})$ / COLE, where W^2 is average bounding box width and L_{maj} is the angle of the best-fit ellipse major axis. Conductivity is high for larger, more vertical pores and when COLE values are low, since those pores remain open even when soil water content approaches saturation.

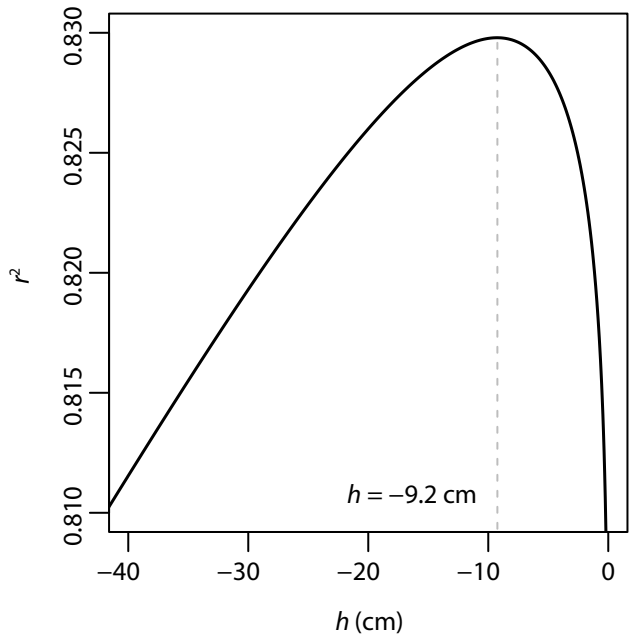

Fig. 7. Plot of coefficient of determination (r^2) of the regression between unsaturated hydraulic conductivity (K) and normalized SSG size as a function of soil water potential (h). The best relationship between K and normalized average SSG size is found when K is calculated at a potential of -9.2 cm.

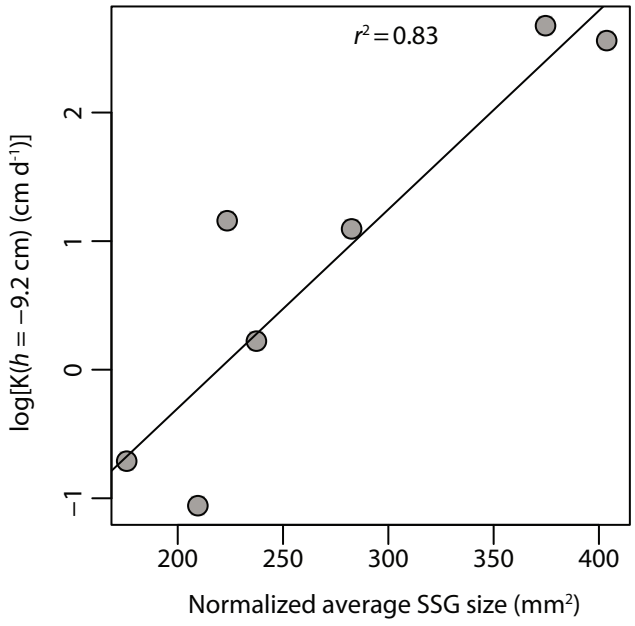

Fig. 8. The relationship between hydraulic conductivity at h = -9.2 cm and normalized average SSG size has a strong positive correlation. Similar to the K_{sat} relationship, large vertically oriented pores with low COLE values are more conductive than horizontal pores or those in areas with high COLE values.

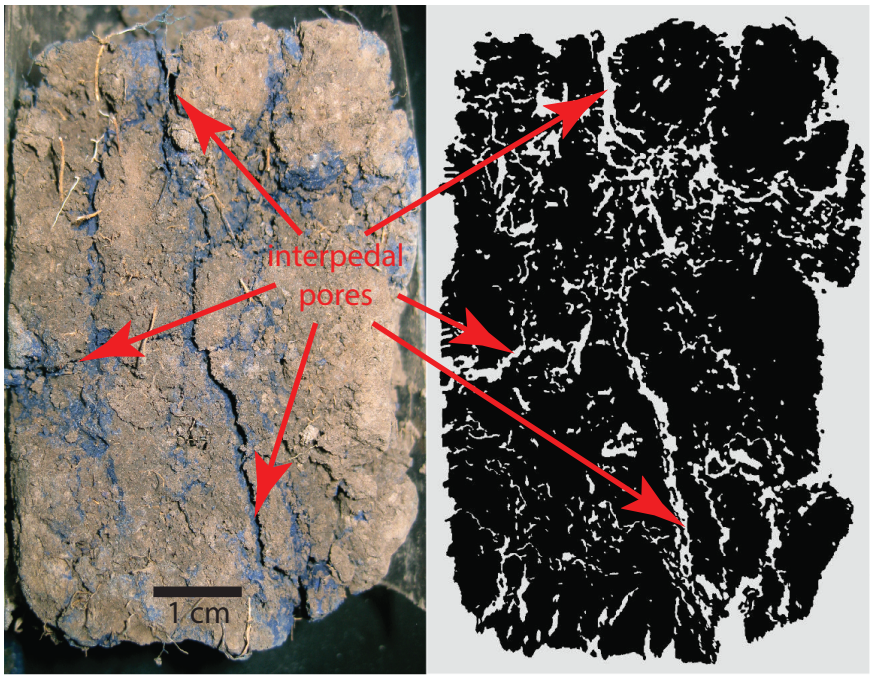

Fig. 9. Visual comparison of dyed core section photograph (left) and MLT scan data (right) demonstrates close agreement between observable conditions and captured digital data. Arrows point out examples where interpedal pores in the core match SSGs in the digital data.

CHAPTER 4. CONCLUSION

Soil structure is commonly recognized as a fundamental soil property that interacts with and partially controls numerous soil morphological, chemical, and transport processes. While its importance is known, it has been a difficult property to describe quantitatively. The relatively recent development of MLT scanning has provided an opportunity to apply the technology to soil profiles in the field with the goal of uncovering meaningful quantitative metrics describing soil structure. MLT scanning has already been used in areas such as ichnology, archaeology, and even determining the bulk density of rocks and soil clods. Prior to this investigation, however, MLT scanning had not been applied to quantifying soil profiles. This work demonstrates solutions to the logistical challenges of using MLT scanning in the field as well as postprocessing requirements for the resulting data. It also illustrates that metrics obtained from the resulting digital data describe soil structure quantitatively. These metrics can then be used to predict soil hydraulic properties. Results of this research provide the opportunity to characterize soil structure on a continuous basis, rather than as a categorical variable, based on physical measurements in the field. While additional study is needed to explore the applicability of these methods to additional sites, these results hold promise for enhancing models of soil water flux by parameterizing structure using field-based soil measurements.

APPENDIX A. LOGISTICS OF MLT FIELD DEPLOYMENT

Field Conditions

Initial attempts to use MLT scanning in the field revealed several challenges. The first issue we encountered was the space requirement in the soil pit. We discovered that excavations needed to be at least 1-m wide to accommodate an operator in the pit for scanner set-up, positional alignment, and adjustments. Deep excavations may require greater width if a telescoping tripod is used to position the scanner, since the extension of tripod legs increases the width of the base. Ambient light, which is known to diminish data quality of structured-light scanners (Voisin et al., 2007), presents another challenge to using MLT in the field. Initially a black cloth was used to block ambient light, covering the scanner and the excavation wall. In addition to blocking ambient light, however, the cloth absorbed heat and minimized air circulation causing the temperature inside the pit to increase. The high temperature occasionally exceeded operational limits of the scanner, which eventually shut down to cool. MLT data was therefore collected at night to avoid interference from ambient light. Nighttime atmospheric conditions also tend to be more stable due to the lack of insolation. This is especially important when collecting data over large areas because conditions at the excavation wall will be generally consistent for a longer time. Thus, heat and evaporative water fluxes at the excavation wall are minimized over the course of the digital data collection by scanning at night.

Preparation of Scan Area

We allowed the excavation wall to dry for 36 hours before scanning to enhance the expression of surface scan gaps (SSGs). We separately tested a core taken a few meters away from the excavation which showed that ~36 hours of drying time (at room temperature) after

saturation was sufficient to produce a strong expression of SSGs within the soil profile. Clay mineralogy in the control section of this soil is classified as smectitic (Soil Survey Staff, 2010) and, while SSGs were easily visible after just 12 hours, they became more pronounced until 36 hours. Additional drying time beyond 36 hours resulted in smaller changes in the interpedal pore expression. This effect is likely to be more pronounced for soils with greater shrink/swell capacity. We recommend at least 36 hours drying time before scanning to strongly express SSGs.

Preparing the excavation wall also presented a challenge for scanning. Shovels, trowels, and soil knives impart distinct artifacts on the wall surface that are detectable in MLT scan data. These artifacts deform or destroy the natural soil structure and can obscure or compact the interpedal pores and other internal structures. The freezing and peeling method using 1,1-difluoroethane (Hirmas, 2013) was developed to diminish or eliminate these effects to the greatest extent possible.

Data Reference and Collection

Alignment of individual scans was previously difficult and time consuming in the absence of easily identifiable reference points. We used colored ball-head pins and tape measures to construct a reference system. Similar to previous work (Lemeš and Zaimović-Uzunović, 2009; Zaimović-Uzunović and Lemeš, 2010), we found that certain colors and surfaces presented difficulties for scanning. Black and white objects were difficult for the scanner to recognize so we used only red, green, yellow, and blue pins and a yellow tape measure. Quickly removing the glossy finish of the pinheads with sandpaper would likely improve their visibility in the point cloud data, as this reflective finish occasionally resulted in

missing data at those points. Presence of a tape measure in the scanned area is critical for data processing, segmenting point cloud data by horizon or by depth, and for maintaining or establishing proper scale and units within the various software programs when the data is post-processed. Placement of the tape measure near the edge of the FOV and the orientation of its concave shape (turned slightly away from the scanner) produced localized shadowing and prevented the scanner from completely collecting the tape in some areas. A flat cloth tape would likely improve visibility in the resulting MLT data over a metal tape, even at the edge of the scanner's FOV. The cloth tape would also provide a matte surface, which would minimize unwanted laser reflection, in contrast to the glossy finish of a metal tape measure. If possible, distance divisions and subdivisions (cm and mm delineations) should be textured (e.g., raised by embroidering) to create depth and more clearly define the delineations in the captured MLT scan data.

REFERENCES

Hirmas, D.R. 2013. A simple method for removing artifacts from moist fine-textured soil faces. Soil Science Society of America Journal. 77:591-593.

Lemeš, S., and N. Zaimović-Uzunović. 2009. Study of ambient light influence on laser 3D scanning. p. 327:330. Proc. ICIT & MPT 2009: 7th International Conference on Industrial Tools and Material Processing Technologies, Ljubljana, Slovenia 2009. ICIT & MPT.

Soil Survey Staff. 2010. Keys to soil taxonomy, 11th ed. Natural Resources Conservation Service, US Department of Agriculture.

Voisin, S., S. Foufou, F. Truchetet, D. Page, and M. Abidi. 2007. Study of ambient light influence for three-dimensional scanners based on structured light. Optical Engineering 46:030502.

Zaimović-Uzunović, N., and S. Lemeš. 2010. Influences of surface parameters on laser 3D scanning. p. D4-026-021:D024-026-024 Proc. 10th International Symposium on Measurement and Quality Control, Osaka, Japan. 5-9 September 2010. International Measurement Confederation.

APPENDIX B. MISCELLANEOUS DATA FROM ANALYSIS AND QUANTIFICATION OF A GRUNDY SOIL (VERTIC ARGIUDOLL)

Fig. B1. NextEngine MLT scanner capturing a photograph of the prepared soil pit face just before performing the MLT scan. The yellow measuring tape on the left side of the photo and colored pins inserted in the excavation wall (not visible) provide a reference system.

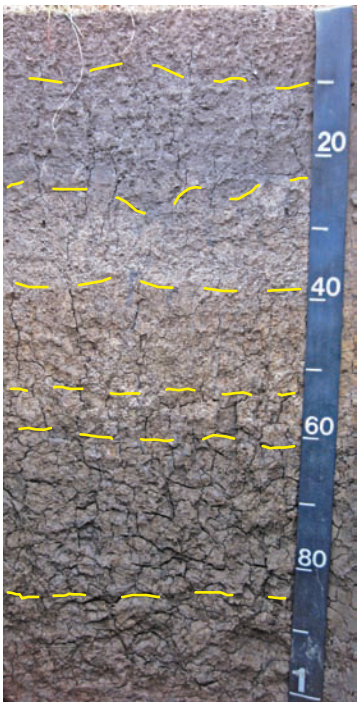

Fig. B2. Photo of soil profile with approximate horizon boundaries.

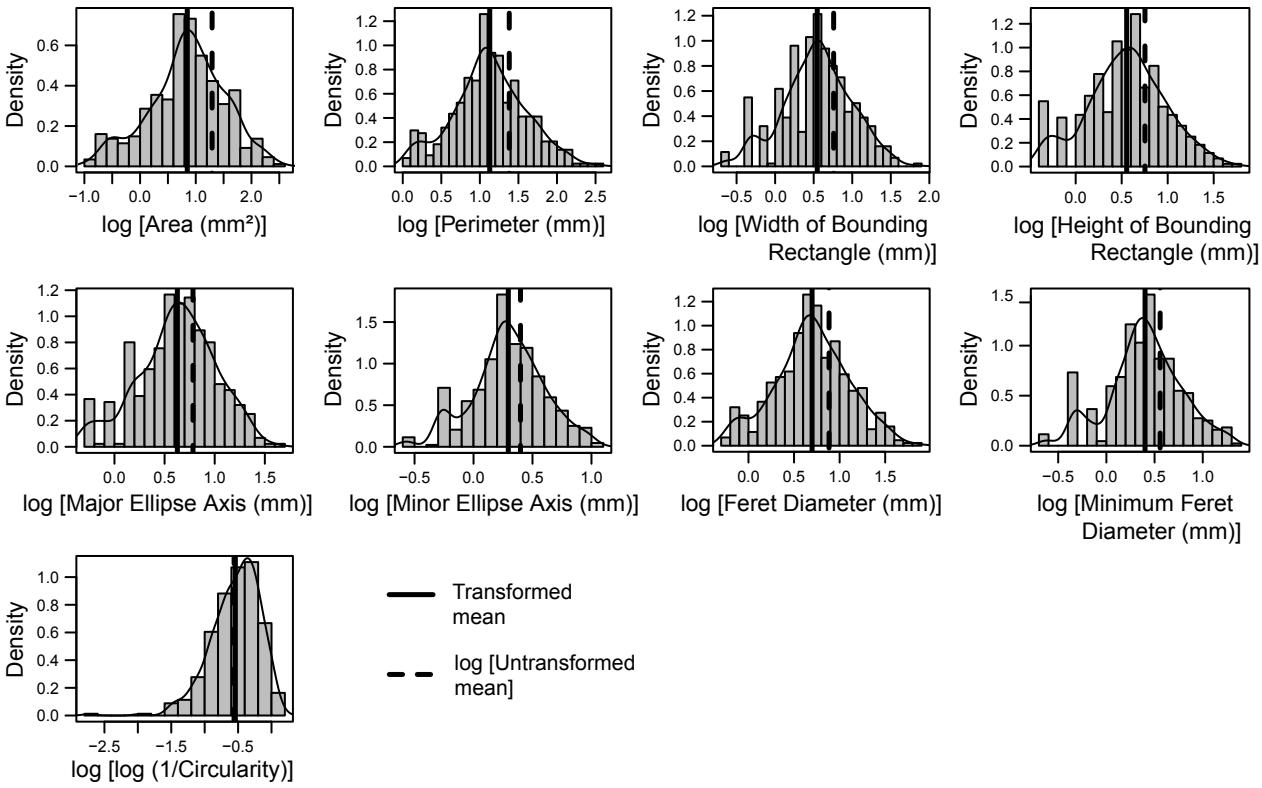

Fig. B3. Histograms of transformed data from a section of the 2Btss2 horizon. Lines show mean values calculated for untransformed data (dashed) and after transformation (solid). In order to display all data on the same scale, the log of the untransformed means are plotted.

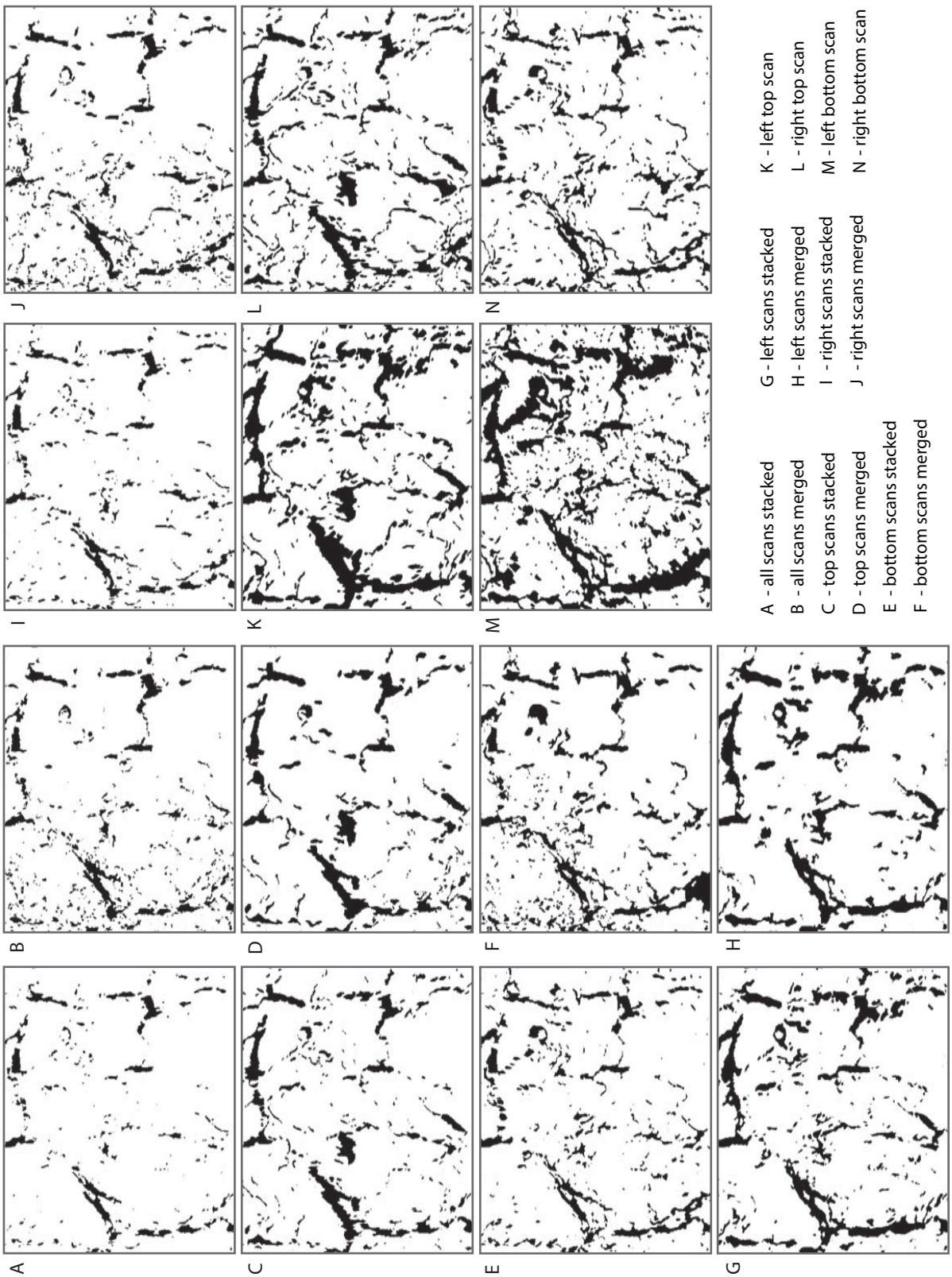

Fig. B4. Binarized scan data (pores in black) of the 14 data configurations of the overlap test projected onto a plane. Each image covers the same 94 mm (width) x 76 mm (height) area within the 2Btss2 horizon.

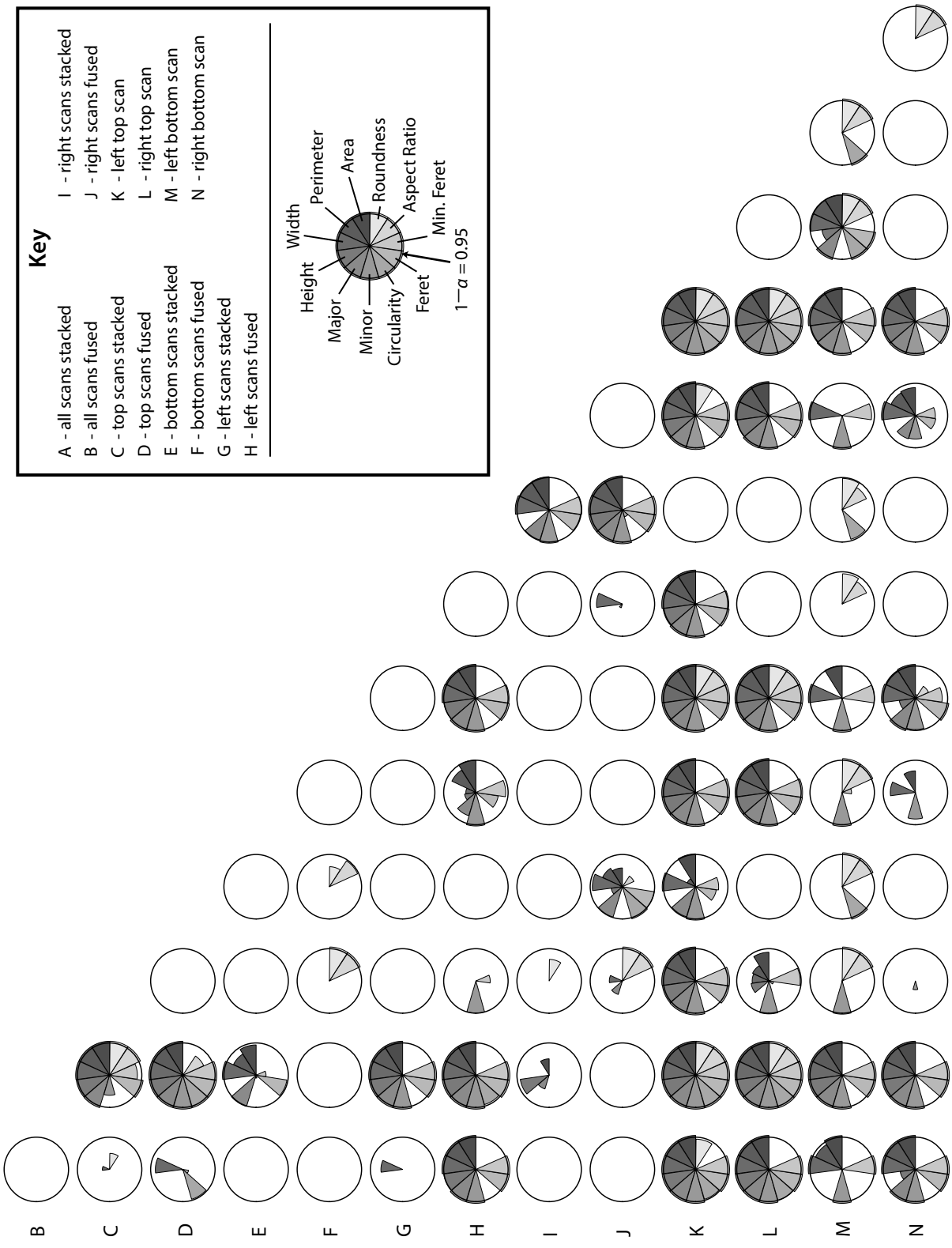

Fig. B5. Star plots displaying 1−*P* values from 11 parameters in 14 overlap configurations. Slices extending to rings or beyond indicate a significant difference between overlap treatments for that variable. Familywise error rate accounted for by the Bonferroni method.

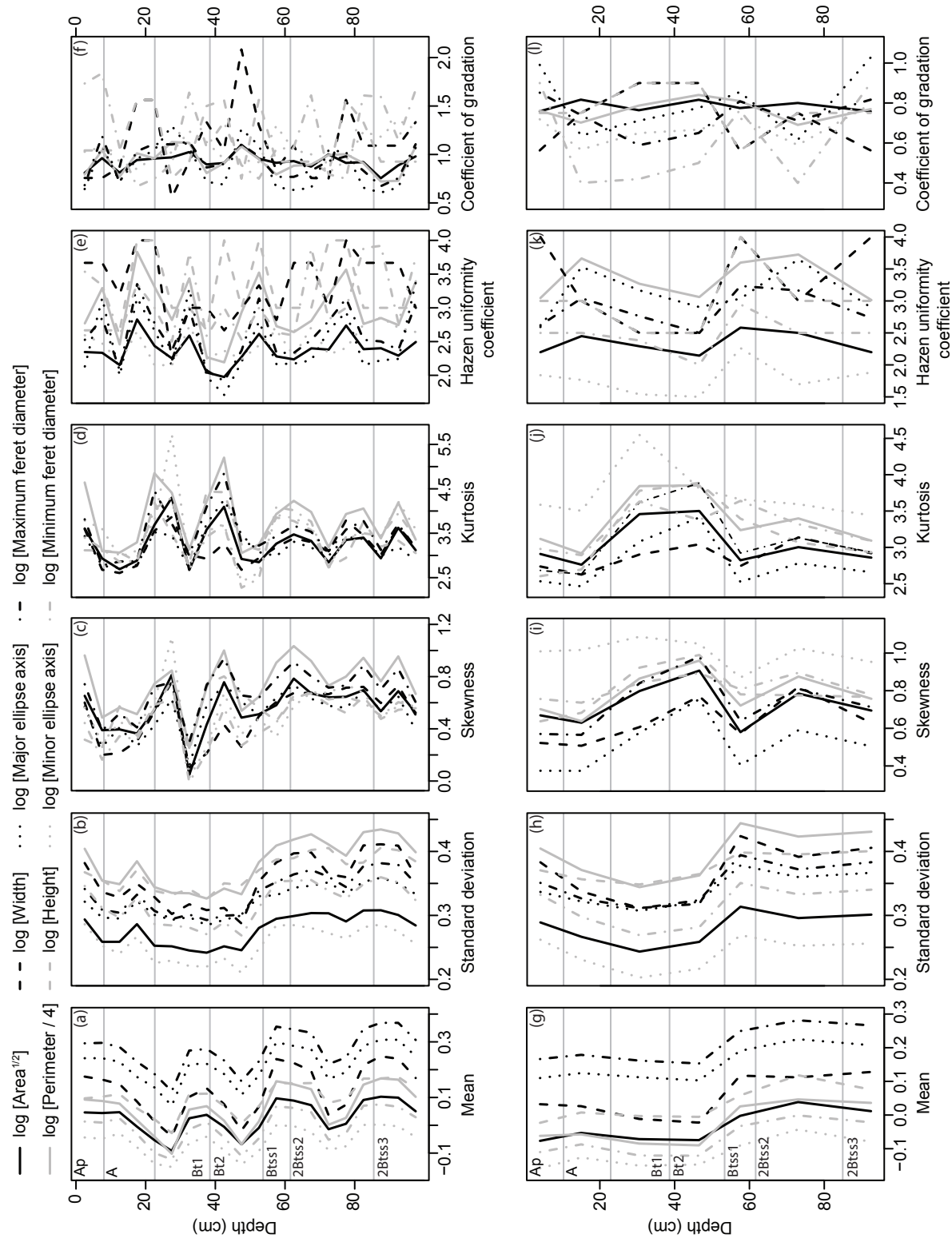

Fig. B6. Statistical moments along with Hazen uniformity coefficient and coefficient of gradation are plotted by 5 cm depth (a-f) and by horizon (g-l). Horizons (gray lines) are labeled in (a). Area and perimeter are given as lengths of equivalent squares ($area^{1/2}$; perimeter/4); units for all metrics are mm. Moments are calculated from log-transformed data. Coefficients of gradation and Hazen uniformity are calculated from untransformed values.

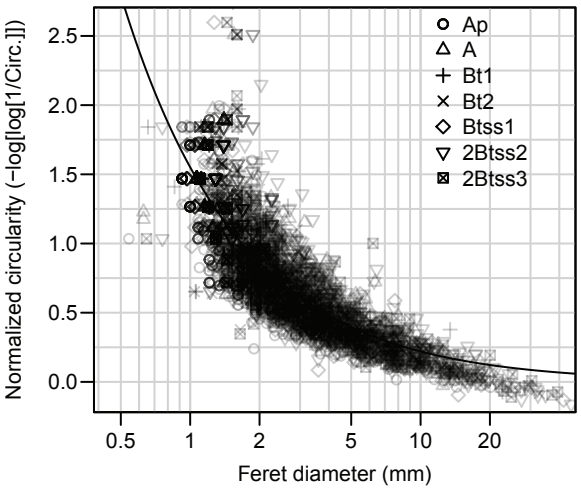

Fig. B7. Normalized circularity (shape) as a function of feret diameter (size) for all measured pores in the profile. Shape of the pores across all horizons is strongly related to size as pores become less circular with increasing size.

Fig. B8. Passive capillary lysimeter installed at study site, including five soil moisture and temperature probes. The drainage control tube (stainless steel) isolates the natural soil structure below most of the root zone.